

University of Alberta

SEISMIC DATA RECONSTRUCTION WITH REGULARIZED LEAST-SQUARES PRESTACK
KIRCHHOFF TIME MIGRATION

by

Abdolnaser Yousefzadeh 

A thesis submitted to the Faculty of Graduate Studies and Research in partial fulfillment
of the requirements for the degree of **Master of Science**.

in

Geophysics

Department of Physics

Edmonton, Alberta
Fall 2008



Library and
Archives Canada

Bibliothèque et
Archives Canada

Published Heritage
Branch

Direction du
Patrimoine de l'édition

395 Wellington Street
Ottawa ON K1A 0N4
Canada

395, rue Wellington
Ottawa ON K1A 0N4
Canada

Your file Votre référence
ISBN: 978-0-494-47448-8
Our file Notre référence
ISBN: 978-0-494-47448-8

NOTICE:

The author has granted a non-exclusive license allowing Library and Archives Canada to reproduce, publish, archive, preserve, conserve, communicate to the public by telecommunication or on the Internet, loan, distribute and sell theses worldwide, for commercial or non-commercial purposes, in microform, paper, electronic and/or any other formats.

The author retains copyright ownership and moral rights in this thesis. Neither the thesis nor substantial extracts from it may be printed or otherwise reproduced without the author's permission.

AVIS:

L'auteur a accordé une licence non exclusive permettant à la Bibliothèque et Archives Canada de reproduire, publier, archiver, sauvegarder, conserver, transmettre au public par télécommunication ou par l'Internet, prêter, distribuer et vendre des thèses partout dans le monde, à des fins commerciales ou autres, sur support microforme, papier, électronique et/ou autres formats.

L'auteur conserve la propriété du droit d'auteur et des droits moraux qui protègent cette thèse. Ni la thèse ni des extraits substantiels de celle-ci ne doivent être imprimés ou autrement reproduits sans son autorisation.

In compliance with the Canadian Privacy Act some supporting forms may have been removed from this thesis.

Conformément à la loi canadienne sur la protection de la vie privée, quelques formulaires secondaires ont été enlevés de cette thèse.

While these forms may be included in the document page count, their removal does not represent any loss of content from the thesis.

Bien que ces formulaires aient inclus dans la pagination, il n'y aura aucun contenu manquant.

■ ■ ■
Canada

To:

my wife:



SAEEDAH

and our little one:



PARSA

Abstract

This thesis examines the problem of designing least-squares Kirchhoff migration algorithms for imaging the subsurface. In particular, the imaging problem is posed as an inverse problem. The forward operator is constructed via a Kirchhoff de-migration operator. Smoothing constraints are used to find a stable solution to the inversion of the de-migration operator.

Numerical strategies (based on semi-iterative solvers) are used to estimate seismic images that are consistent with measured wave fields. The algorithm, denoted Least-squares PreStack Time Migration (LS-PSTM), is used to estimate common image gathers (CIG) with reduced acquisition artifacts. The algorithm is also capable of regularizing the data, in other words, it can be used to reconstruct missing seismograms.

Synthetic and real data examples are used to validate theoretical findings and test the performance of the proposed LS-PSTM algorithm.

Acknowledgements

This thesis would not have been possible without the support of many people.

First and foremost, I wish to express my gratitude to my supervisor, *Prof. Mauricio D. Sacchi*, for his teaching, supervision, guidance and tremendous patience. I also wish to thank him for spending his valuable time to read, correct and comment on my thesis. I believe I will greatly benefit from his vast knowledge of seismic inversion and imaging, in my future research and work.

I extend my thanks to the members of my examining committee for their valuable suggestions and for agreeing to read my thesis.

I also would like to thank my colleagues in SAIG who made the office a friendly environment, especially Mostafa Naghizadeh, Sam Kaplan and Somanath Misra for precious technical discussions and suggestions.

My work made use of the infrastructure and resources of AICT (Academic Information and Communication Technologies) of the University of Alberta. The author would like to convey thanks to the AICT Research Group for providing computer facilities, training courses, and answering his questions.

My gratitude goes out to my sponsor, Institute of Petroleum Engineering of University of Tehran, IRAN. Many thanks go in particular to my friendly teachers in the Institute of Geophysics at the University of Tehran: Dr. Hamid-reza Siahkoohi, Dr. Majid Nabibidhendi, and Dr. Mohammad-ali Riahi.

The author wishes to express his love and gratitude to his and his wife's beloved families in IRAN, for their understanding and endless love.

Finally, special thanks are due to my wife, *Saeedeh Abbaszadeh*, for her unflinching patience, support, encouragement, understanding, and always having confidence in me during these arduous years of study.

Contents

1	Introduction	1
1.1	Background	1
1.2	Least-Squares migration	4
1.3	Overview of the data reconstruction problem	5
1.4	Scope of this thesis	6
1.5	Outline of this thesis	6
2	Kirchhoff Time Migration and Modeling	8
2.1	Wave equation and Kirchhoff migration	8
2.2	Kirchhoff migration and modeling in the time-domain	10
2.2.1	Forward and adjoint operators in midpoint offset space	14
2.3	Implementation of Kirchhoff time migration/modeling	15
2.3.1	Migration weight	15
2.3.2	Migration aperture	15
2.3.3	Spatial anti-aliasing of the migration operator	20
2.3.4	Pseudocode for Kirchhoff time migration/modeling	23
2.4	Summary	25
3	Seismic Data Migration and Inversion	27
3.1	Discrete inverse theory	27
3.2	Kirchhoff LS-PSTM	28
3.3	Regularized Kirchhoff LS-PSTM	30
3.3.1	The Method of Conjugate Gradients (CG)	32
3.4	Summary	35

4	LS-PSTM for Resolution and Regularization of Incomplete and Irregular Data	36
4.1	Migration of incomplete synthetic data	36
4.2	LS-PSTM of incomplete data	40
4.2.1	Offset dependent regularized LS-PSTM of incomplete data	40
4.3	Data reconstruction by LS-PSTM	47
4.3.1	Synthetics examples of data reconstruction via LS-PSTM	48
4.4	LS-PSTM and data reconstruction of the Marmousi data set	51
4.5	Dependency of LS-PSTM data reconstruction on velocity information	55
4.6	Summary	55
5	PSTM, Regularized LS-PSTM and Data Reconstruction of Real Data	59
5.1	Gulf of Mexico data set	59
5.2	Velocity analysis and multiple attenuation	61
5.2.1	Parabolic Radon Transform	61
5.3	PSTM and LS-PSTM and reconstruction prior to multiple attenuation	63
5.4	Regularized LS-PSTM and data reconstruction after multiple attenuation	72
5.5	Summary	73
6	Discussion and Conclusions	80
6.1	Future work	81
	References	82

List of Figures

1.1	Positioning error for dipping reflectors. The true reflector A will be mispositioned in the seismic section and appear as the reflector A'	2
2.1	Implementation of aperture in Kirchhoff PSTM. a) A triangular aperture. b) A combination of triangle and constant aperture. For each trace in the midpoint position, Kirchhoff summation is applied on samples in the area inside the aperture.	17
2.2	Fresnel zone for a wave with wavelength= λ is equal to the distance of m_1m_2	17
2.3	Fresnel zone for an offset section after Sun and Bancroft (2001). Here, x_f is Fresnel zone radius and t_h is the offset traveltime h is half source-receiver distance.	20
4.1	Synthetic model used to test PSTM and LS-PSTM. a) Reflectivity model. b) Velocity model. The vertical bar indicates compressional seismic velocities in m/s	37
4.2	a) Synthetic data generated from the reflectivity model in in Figure (4.1) displaying 125 traces from one shot gather. b) Seismic image generated via Kirchhoff PSTM.	38
4.3	Migration with missing observations. a) and b) Decimated data with 75% of data removed and PSTM. c) and d) Decimated data with 90% of data removed and PSTM.	39
4.4	With incomplete data, resulted LS-PSTM has more resolution than standard migration and is comparable with the original model as in Figure (4.1). a) LS-PSTM when 50% of data is randomly removed. b) 90% of data is removed.	41
4.5	Convergence of LSCG method when only 10% of data is present.	43
4.6	Effect of using regularized LS-PSTM on the estimation of common image gathers. Each gather corresponds to one midpoint position and 10 offset bins. a) CIG of PSTM. b) CIG of regularized LS PSTM with $\mu = 1$, c) $\mu = 10$, and d) $\mu = 150$	44

4.7	Effect of using offset dependent regularized LS-PSTM on the stack images. Each image is obtained by stacking common image gather along the offset dimension.	
	a) Without regularization ($\mu = 0$), b) $\mu = 1$, c) $\mu = 10$, and d) $\mu = 150$.	45
4.8	Convergence of offset dependent regularization LS-PSTM when 90% of the data are missing as a function of trade-off parameter μ .	46
4.9	Data reconstruction by offset dependent regularized LS-PSTM for the synthetic model of Figure (4.1). a) Original data. b) Decimated data with 90% of the data removed. c) The reconstructed data. d) Error panel or difference between original and reconstructed data.	49
4.10	RMS error for data reconstruction by offset dependent regularized LS-PSTM for the synthetic model of Figure (4.1) versus trade-off parameter, μ . The best data reconstruction is obtained when $\mu = 150$. The reconstructed data are shown in Figure (4.9).	50
4.11	The Marmousi synthetic model. a) Velocity model. b) Image obtained by migrating the decimated data with PSTM. c) Image obtained by migrating the decimated data with LS-PSTM.	53
4.12	Data reconstruction for Marmousi data set. a) Original data, in this case field record 230. b) Decimated data with 50% of traces removed. c) Reconstructed data. d) Error panel or difference between original data and reconstructed data.	54
4.13	Effect of inexact velocity information on Kirchhoff PSTM. a) 10% velocity error. b) -10% velocity error. The image obtained with the correct velocity model in displayed in Figure (4.2 b)	57
4.14	Effect of inexact velocity information on data reconstruction. a) Reconstructed data with 10% velocity error. b) Reconstructed data with -10% velocity error. Error panels for a) and b) are shown in panels c) and d), respectively.	58
5.1	Stacked section of the Gulf of Mexico data set. Processed with the Seismic Unix software prior to multiple attenuation. Strong first order multiples are visible at 3.2, 3.7, 4.4, and 5sec in the middle and right-hand side of image. After 6 sec another series of multiples are visible.	60

5.2	Velocity analysis using semblance analysis for the CDP 2100 from the Gulf of Mexico data set. a) Velocity analysis of the original data. b) Velocity analysis of the data after removing multiples using the Radon transform.	64
5.3	Multiple removal from the Gulf of Mexico data set, field record 647. a) Original data with strong multiples. b) NMO corrected data. c) Data after multiple attenuation. d) Data after inverse NMO correction.	66
5.4	Migration images of the Gulf of Mexico data set with 50% of shot records removed. a) PSTM subsurface image. b) LS-PSTM image.	67
5.5	Data reconstruction of Gulf of Mexico data set. Multiples are present in the original data. a) The original data displaying shotgather 647. b) Decimated data. c) Reconstructed shot gather. d) Difference between original and reconstructed data.	68
5.6	Comparison between multiples and un-constructed events in the process of data reconstruction of the row data. Field record 647, a) Estimated multiples using RT (the differences between original data (Figure 5.3 a) and demultiplied data by RT (Figure 5.3 d)). b) Un-constructed events in the data reconstruction (Figure 5.5 d). c) Difference between a) and b).	69
5.7	CIG of CDP 2100 of the Gulf of Mexico data set. The multiples show themselves as parabolic events, therefore performing smoothness in the offset direction is not effective. a) PSTM. b) LS-PSTM.	71
5.8	Migration images of the Gulf of Mexico data set after multiple attenuation using 50% of the shot records. a) PSTM. b) LS-PSTM.	74
5.9	Data reconstruction of the Gulf of Mexico data set after multiple removal with parabolic Radon Transform. a) Original data. b) Decimated data c) Reconstructed data. d) Difference between original data and reconstructed data.	75
5.10	CIG of CDP 2100 from data after multiple removal. a) PSTM. b) LS-PSTM. c) LS-PSTM with offset dependent regularization with $\mu = 100$ and d) with $\mu = 2000$	76
5.11	Regularized LS-PSTM images of the Gulf of Mexico data set after multiple attenuation. a) Offset dependent regularized LS-PSTM with $\mu = 100$ and . b) $\mu = 2000$	77

5.12	Data reconstruction of the Gulf of Mexico data set after multiple attenuation with offset dependent LS-PSTM. a) $\mu = 100$. b) Difference between original data and reconstruction with $\mu = 100$. c) Reconstructed data using regularized LS-PSTM with $\mu = 2000$. d) Difference between original data and reconstruction with $\mu = 2000$	78
5.13	RMS error for data reconstruction by offset dependent regularized LS-PSTM for the Gulf of Mexico data set versus trade-off parameter, μ . The data reconstruction is not improved by introducing smoothness.	79

List of symbols and abbreviations

Numerics

ΔP trace spacing

P maximum stepout

ω angular frequency

Hz Hertz

T period

G Green's function

h_s source sampling function

h_r receiver sampling function

h offset

\mathcal{R} regularization function

R Fresnel zone radius

r ramp function

θ_r incident angle

V wave velocity

v volume

sec second(s)

L forward modeling operator

m earth reflectivity model vector

m₀ real earth reflectivity model vector

m̂ migration image

n additive or environmental noise

d (seismic) data vector

J cost function

N length of triangle smoothing operator or
Number of the unknown data

Wg weight function

\mathcal{W} weight function

W wavelet function

D_{1h_x} first order derivative operator along
the offset direction

D_{2h_x} second order derivative operator along
the offset direction

μ trade-offset parameter for inversion

δ delta function

τ (zero-offset) travelttime

t travelttime

$\tau_{x_s,0,x,z}$ travelttime from source to image point

$\tau_{x,z,x_r,0}$ travelttime from receiver to image
point

ψ acoustic wavefield

Abbreviations

AVA Amplitude Versus Angle

AVAz Amplitude Versus Azimuth

AVO Amplitude Versus Offset

AVP Amplitude Versus ray Parameter

CG Conjugate Gradients

CIG Common Image Gather(s)

CDP Common DepthPoint

DMO Dip MoveOut

DSR Double Square Root

EAGE European Association of Geoscientists and Engineers

FT Fourier Transform

LS Least-Squares

LSCG Least-Squares Conjugate Gradients

LSM Least-Squares Migration

NMO Normal MoveOut

OBS Ocean Bottom Seismic

PSPI Phase Shift Plus Interpolation

PSTM PreStack Time Migration

RMS Root Mean Squares

RT Radon Transform

SAIG Signal Analysis and Imaging Group

SEG Society of Exploration Geophysicists

TWT Two-Way Traveltime

Chapter 1

Introduction

1.1 Background

Reflection seismology is a geophysical prospecting method used for hydrocarbon reservoir exploration, geotechnical studies, and imaging the earth's crust. In this method, a source or array of sources releases energy in the form of elastic waves. The energy propagates down into the earth and is reflected back by geological interfaces. The reflections are acquired and processed to form a model of the subsurface.

The recorded data may contain unwanted events and suffer from acquisition problems. It is important to mention that not all the data can be recorded. In general, logistic and economical constraints often dictate the amount of data that one can collect.

In order to form a model of the subsurface, the goal of exploration seismology, collected raw data must undergo a seismic processing flow. In seismic data processing, random noise and unwanted deterministic signals are removed to obtain a data set rich in reflected energy. The data are then processed to account for the geometrical position of sources and receivers, and to improve the signal-to-noise ratio. For instance, the effect of source and receiver distance for a given seismogram is removed via the step called "Normal MoveOut (NMO) correction". The resulting data corresponds to seismograms that mimic an acquisition where the source-receiver distance was reduced to zero. Stacking (averaging) seismograms corresponding to the same reflection point in the subsurface leads to the stack section. This is an image of the subsurface displaying the position of geological interfaces in time. The main assumption in the aforementioned process is that the reflectors are horizontal, or in another words, the earth is horizontally homogeneous.

1.1. BACKGROUND

In the real world, however, layering in the crust does not conform a horizontally stratified model. Dips of layers need to be considered and the typical image of the subsurface gained via the seismic section is incorrect as we will illustrate.

When reflected wave fields arise from a dipping layer as shown in Figure (1.1), the real reflector point is denoted by **CDP**, (Common Depth Point) and the corresponding trace (seismogram) must be placed in the position **SR2**. However, conventional methods of seismic processing places the trace in the position **SR1**, in the middle of **S** and **R**. As a result, the final zero-offset seismic section will show the dipping layer **A** as **A'**. The mispositioned reflector **A'** underestimate the real dip of the reflector **A**. A solution to this problem is to apply a "*migration*" algorithm to put reflectors in their correct spatial position.

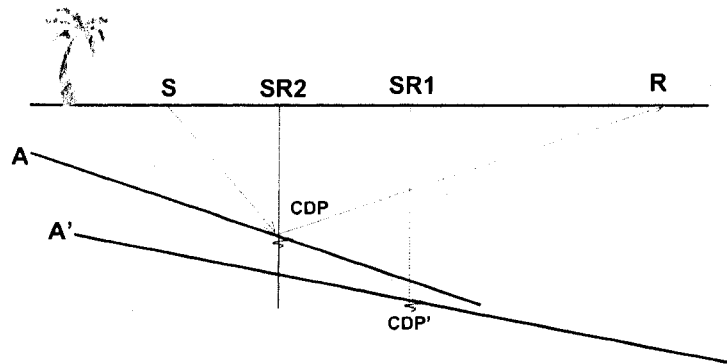


Figure 1.1: Positioning error for dipping reflectors. The true reflector **A** will be mispositioned in the seismic section and appear as the reflector **A'**.

Migration not only moves reflection events to their true spatial positions with true amplitudes and dips but also collapses the diffracted signal back to scattering points in the seismic section. Migration transforms a time section seismic wavefield, recorded on the earth surface, to an earth reflectivity map which can be expressed as surface position versus depth (depth migration) or surface position versus time (time migration).

The history of migration goes back to 1920s, when mechanical migration on data were done by hand. Hagedoorn (1954) introduced the method of diffraction summation. The primary methods were based on the concept of ray tracing and scalar diffraction theory.

In the beginning of 1970s John Claerbout and his colleagues at the University of Stanford introduced migration as an approximate solution to the wave equation (Claerbout and Doherty, 1972). It was the first link between migration and the wave equation. The idea was that a zero-offset seismic section can be modeled as an upgoing zero offset wavefield produced by exploding reflectors. In this model migration is considered as downward continuation followed by imaging. Because downward wavefield continuation is conveniently implemented via the finite difference solution to the scalar wave equation, this method of migration is called "finite difference migration".

Schneider (1978) introduced Kirchhoff wave equation migration. He showed that by ignoring multiples and with proper scaling and filtering, the diffraction summation method is an exact solution to the wave equation. Shortly after that, Gazdag (1978) and Stolt (1978) showed that the migration sum can also be obtained via Fourier transform methods. For instance, Stolt's (1978) method is a coordinate transformation from frequency to vertical wavenumber. Gray et al. (2000) summarized the history of migration and provides a good survey of methods often used by the oil/gas exploration industry.

In the method of Kirchhoff migration each point in the image domain is considered a diffractor point. This method tries to collapse all diffracted energy back to the scatterer point. In the resulting image each dipping reflector is moved to the correct location with the true dip and length. The Kirchhoff migration method is not able to deal with multipathing rays. It has many advantage, however, such as efficiency and low cost, the ability to handle irregularly sampled data, adapt well to prestack or poststack volumes, work with converted waves, and allows data aliasing to be controlled, to name a few.

For a simple structural model, Kirchhoff migration of regular and dense (high subsurface foldage) seismic data with long aperture often gives acceptable images of the subsurface. In reality, however, well-sampled data are often difficult to obtain. Economical aspects, human made obstructions, geographical obstacles (rivers, lakes) and environmental regulations often leads to data that are not sampled according to theoretical needs. In the marine case, steamer feathering due to water currents un-parallel to in-line

direction, acquisition interruptions due to severe storms, etc, can also lead to data sets with missing or poorly positioned data on a regular grid.

1.2 Least-Squares migration

Methodologies to overcome the aforementioned shortcomings of standard Kirchhoff migration can be managed by approximating the exact inverse by a generalized inverse as proposed by Tarantola (1984) and studied by many other researchers (LeBras and Clayton (1988), Beydoun and Mendes (1989), Lumley and Beydoun (1997), Nemeth et al. (1999), Nemeth et al. (2000), Duquet et al. (2000), Xu et al. (2001), Kuehl and Sacchi (2001b) and Kuehl and Sacchi (2003)). We often refer to this approach the Least-Squares Migration (LSM) algorithm. LSM has been used as a method to overcome many problems in seismic imaging such as migration of irregular data, removing coherent noise, removing migration artifacts, and true amplitude AVA (Amplitude Versus Angle)/AVO (Amplitude Versus Offset) analyzes. LSM is computationally expensive and consequently, it has not become a standard method to process seismic data.

We can consider two classes of LSM algorithms: first those Kirchhoff type proposed by Nemeth et al. (1999) and Duquet et al. (2000), and wave equation types proposed by Kuehl and Sacchi (2001b). In the LSM algorithm, the forward modeling operator builds data from a subsurface reflectivity model using a method such as Kirchhoff diffraction forward modeling. The image of the reflectivity is found by numerically finding a solution to the inverse of the de-migration operator.

Nemeth et al. (1999) and Nemeth et al. (2000) showed that LSM can reduce seismic artifacts arising from data sampling problems.

LSM is not limited to the Kirchhoff or wave equation migration and can be used with any other migration method such as Fourier transform methods. Methods based on wave equation migration have higher cost compare to the Kirchhoff method. Kuehl and Sacchi (Kuehl and Sacchi (2001a) , Kuehl and Sacchi (2001b) and Kuehl and Sacchi (2003)) used wave equation LSM methods to migrate incomplete data and for AVP (Amplitude Versus ray Parameter) and AVA inversion. Wang and Sacchi (2007) also added a sparseness constrain to wave equation LSM to enhance vertical resolution of CIG for AVP studies.

1.3 Overview of the data reconstruction problem

In seismic methods, the recorded data are the discrete version of a continuous 3D elastic wavefield. A perfect wavefield sampling is impossible in the real world and the recorded seismic data always suffer from incompleteness and irregularity.

Irregularity in the seismic data is a direct result of data acquisition. Data acquisition is the most expensive and time consuming part of seismic surveying. Rivers, swamps, jungles, and human-made structures cause un-even distribution of sources and receivers. This is due to economical and environmental aspects on land, especially in 3D data acquisition.

In the case of marine data gathering, irregularity and incompleteness of the data are results of streamer feathering (especially in far offsets), marine traffic, well-sites, etc. Also in the case of 3D marine data acquisition, the lack of wide-azimuth information and missing near offset data is inevitable. Missing or unreadable tapes and bad-trace muting are considered another sources of data irregularity.

The problem of irregularity in seismic data affects many processing steps such as: multiple attenuation, full 3D wave-equation imaging and AVO/AVA/AVAz (Amplitude Versus Azimuth) studies, 4D seismic monitoring, and resolution enhancement.

Multiple attenuation is an important step in seismic data possessing. The Gulf of Mexico data set is an example of the previous statement (Chapter 5). There are many methods for multiple elimination. Some of the most effective methods need regular data sampling. For these methods, data reconstruction with regular and complete positions of sources and receivers is necessary.

Wave equation migration solves the acoustic wave equation in the frequency domain and needs regular sampling of data. Usually missing data are replaced by zeros and consequently they will introduce artifacts in the final image. Using the method of least-squares wave equation migration is a computationally expensive solution to the problem. Using methods that are less expensive and less dependent to the velocity, for example Kirchhoff Least-squares PreStack Time Migration (LS-PSTM), for data reconstruction prior to the wave equation migration can decrease the computational cost.

Regular distribution of offsets/azimuths is vital information for AVA and AVAz anal-

ysis for reservoir characterization.

4D reservoir monitoring compares two or more 3D (or 2D) seismic images of subsurface. Positioning sources and receivers in the same locations as the previous 3D (or 2D) is only possible in the Ocean Bottom Seismic (OBS) surveying. In order to properly put newer seismic images with older ones, side by side, different acquisition geometries must be transferred to one acquisition geometry.

Kirchhoff prestack migration of incomplete/irregular data results artifacts in the migrated image (Gardner and Canning, 1994).

In this thesis, I simulated the incompleteness of data by purposely removing some traces or shot gathers prior to imaging. Removing parts of data allows measurement of the performance of the algorithm for resolution improvement and data reconstruction. When the data reconstruction is perfect, the difference between the original data and reconstructed data must include only random noise.

However, It is emphasized that Kirchhoff LS-PSTM algorithm is not effective in an areas with complex geological structures, for example in the Marmousi data set (Chapter 4). Data reconstruction via Kirchhoff LS-PSTM is less expensive than a depth migration implementation and also it is less sensitive to the velocity model than depth imaging. Therefore it can be performed for data regularization and reconstruction prior to the more expensive, depth imaging methods.

1.4 Scope of this thesis

This thesis focuses on constrained Least-Squares PreStack Time Migration (hereinafter called "LS-PSTM") of the Kirchhoff type. In particular, I will discuss implementation issues, and the impact on resolution for the case of irregularly sampled data.

1.5 Outline of this thesis

In Chapter 2 the basic theory of Kirchhoff integral migration/ modeling and practical aspects of operator design are reviewed. The implementation of Kirchhoff migration with amplitude preserving weights, anti-aliasing and aperture limitation is presented.

1.5. OUTLINE OF THIS THESIS

In Chapter 3 I present LS-PSTM and I introduce a offset-dependent regularization strategy that helps to overcome sampling and migration artifacts.

In chapter 4 the applications of LS-PSTM to the problem of seismic data reconstruction is studied.

Chapter 5 deals with problems associated with LS-PSTM and data reconstruction of a Gulf of Mexico data set contaminated with strong multiple reflections.

Finally, Chapter 6 concludes the thesis and provides recommendations for future work.

Chapter 2

Kirchhoff Time Migration and Modeling

2.1 Wave equation and Kirchhoff migration

Helmholtz scalar acoustic wave equation in the frequency domain is given by

$$\nabla^2 \psi(x, \omega) + \frac{\omega^2}{V^2} \psi(x, \omega) = S(x, \omega), \quad (2.1)$$

where ψ is the seismic wavefield in the frequency domain, ω is angular frequency, V is speed of sound, x is position and S denotes source wave function (Morse and Feshbak, 1953).

The wavefield ψ is composed of a downgoing wavefield D and an upgoing wavefield U . For a source point at x_s , the downgoing wavefield at any location x inside the volume v under the recording surface can be expressed by the following equation in the frequency domain (Audebert et al., 1997):

$$D(x, \omega|x_s) = \int_v G(x, \omega|x') S(x', \omega|x_s) dx', \quad (2.2)$$

where $G(x, \omega|x')$ is the Green function solution to the scalar wave equation (2.1) at x with source at x' , and $S(x', \omega|x_s)$ is the source function at x' , given point source at x_s . Neglecting the absolute amplitude of source, assuming that the source has a delta function shape in time and space, $\delta(t)\delta(x' - x_s)$, and considering that the downgoing wavefield contains only primary arrivals from the source (Audebert et al., 1997):

2.1. WAVE EQUATION AND KIRCHHOFF MIGRATION

$$D(x, \omega|x_s) \approx \int_v G(x, \omega|x') \delta(t) \delta(x' - x_s) dx' = G(x, \omega|x_s), \quad (2.3)$$

which means that the downgoing wavefield can be reconstructed by forward modeling with the Green function (Lumley, 1989).

On the other hand, the upgoing wavefield, contains only primary energy reflected back from the reflection point x and recorded by the receiver at position x_r , is obtained by space-frequency integration over the recorded boundary data, weighted by the normal derivative of the Green function:

$$U(x, \omega|x_s) = \int_s \hat{n} \cdot \nabla G(x_r, \omega|x) \psi(x_r, \omega|x_s) dx_r, \quad (2.4)$$

where s is recording surface enclosing v , $G(x_r, \omega|x)$ is receiver Green function, \hat{n} is a normal vector to the recording surface, and ∇ is the gradient operator to x along the recording surface at $x = x_r$.

The dynamic imaging condition approximates the upgoing wavefield via the convolution of the earth reflectivity $R(x)$ with the downgoing wavefield $D(x, \omega)$ (Claerbout, 1971):

$$U(x, \omega) = R(x)D(x, \omega), \quad (2.5)$$

where $R(x)$ is weighted zero-lag cross-correlation of the source and the reflected wavefields, normalized by the local energy of the source wavefield, DD' :

$$R(x) \approx \sum_{\omega} \mathcal{W} U D' \approx \sum_{\omega} \frac{U(x, \omega) D'(x, \omega)}{D(x, \omega) D'(x, \omega)}, \quad (2.6)$$

here \mathcal{W} represents the migration weight which using equation (2.3) can be estimated via (Audebert et al., 1997):

$$\mathcal{W}^{-1} = DD' \approx G(x, \omega|x_s) G'(x, \omega|x_s) = |G(x, \omega|x_s)|^2. \quad (2.7)$$

The cross-correlation imaging condition evaluated at zero-lag, prevents instability in the reflectivity when the downgoing wavefield is weak. It distorts the true amplitude response but enhances stability (Claerbout, 1971).

2.2. KIRCHHOFF MIGRATION AND MODELING IN THE TIME-DOMAIN

By averaging weighted versions equation (2.6) over all single shot-profile, the reflectivity or *Kirchhoff migration* in the frequency domain has the following form (Audebert et al., 1997):

$$m(x) = R(x) \approx \int_{\omega} \int_{x_s} \int_{x_r} \mathcal{W}[\hat{n} \cdot \nabla G(x_r, \omega|x)] G'(x, \omega|x_s) \times \psi(x_r, \omega|x_s) dx_r dx_s d\omega. \quad (2.8)$$

Assuming sources and receivers located on the earth surface $z = 0$ and a reflection point at depth of z , (2.8):

$$G(x_r, \omega|x) \approx A_{xr} e^{-i(\omega\tau_{x,z,x_r,0} + \phi_r)}, \quad (2.9)$$

and

$$G(x_s, \omega|x) \approx A_{sx} e^{i(\omega\tau_{x_s,0,x,z} + \phi_s)}. \quad (2.10)$$

where A_{ij} , $\tau_{i,j}$ and ϕ_i are the WKB amplitude factors, traveltimes and phase rotations for a single arrival Green function from i to j .

Prestack Kirchhoff migration in the frequency domain (Equation 2.8) can be converted to a time domain equation by performing an inverse temporal Fourier transform on it (Audebert et al., 1997):

$$m(x) \approx \int_{x_s} \int_{x_r} \cos \theta_r \mathcal{W} e^{i(\phi_s + \phi_r)} \hat{d}(x_s, x_r, t = \tau_{sr}) dx_r dx_s, \quad (2.11)$$

where θ_r is incident angle at each receiver position, $\cos \theta_r$ is the obliquity factor, and \hat{d} is τ_{sr} time shifted data. Using WKB approximation, equation (2.11) can be easily used for Kirchhoff prestack migration.

In the next section an efficient time-domain version of migration equation (2.8) and its adjoint with some of their practical aspects are introduced.

2.2 Kirchhoff migration and modeling in the time-domain

Kirchhoff seismic modeling in the time-domain can be stated by equation (Nemeth et al., 1999):

2.2. KIRCHHOFF MIGRATION AND MODELING IN THE TIME-DOMAIN

$$d(x_s, x_r, t) = \int m(x, z) W(t) * G(x_r, 0, t|x, z) * \ddot{G}(x, z, t|x_s, 0) dx dz, \quad (2.12)$$

where $d(x_s, x_r, t)$ are the observed data on the earth surface, ($z = 0$), and x_s and x_r are the position of source and receiver along the seismic line, respectively. The earth reflectivity is denoted by $m(x, z)$, $W(t)$ is the source wavelet, and $G(x_r, 0, t|x, z)$ and $G(x, z, t|x_s, 0)$ denote the time-domain Green functions from reflector point (x, z) to the receiver location and from source location to the reflector point (x, z) , respectively, and \ddot{G} denote the second derivative of Green function.

Using zeroth order asymptotic Green functions, the Green functions are given by

$$G(x, z, t|x_s, 0) = A_{sx} \delta(t - \tau_{x_s, 0, x, z}), \quad (2.13)$$

$$G(x_r, 0, t|x, z) = A_{xr} \delta(t - \tau_{x, z, x_r, 0}), \quad (2.14)$$

where $\tau_{x_s, 0, x, z}$ and $\tau_{x, z, x_r, 0}$ are the traveltimes from the reflection point to source and receiver, respectively. The traveltimes are computed via ray tracing and or via numerical solution of the Eikonal equation (Reshef and Kosloff (1986), Vidale (1988), and Gray and May (1994)). The weights A_{sx} and A_{xr} are WKB amplitude terms that can be computed by solving the Transport equation (Bleistein (1984) and Cerveny (1985)).

In a constant velocity medium, the travel-times have simple analytical forms:

$$\tau_{x_s, 0, x, z} = \sqrt{\frac{(x_s - x)^2}{V^2} + \frac{z^2}{V^2}}, \quad (2.15)$$

and

$$\tau_{x, z, x_r, 0} = \sqrt{\frac{(x_r - x)^2}{V^2} + \frac{z^2}{V^2}}. \quad (2.16)$$

After combining Green functions, the forward equation in the time-domain can be written as follows: (Nemeth et al., 1999):

$$d(x_s, x_r, t) = \int \int m(x, z) A_{sx} A_{xr} \ddot{W}(t - \tau_{x_s, 0, x, z} - \tau_{x, z, x_r, 0}) dx dz. \quad (2.17)$$

2.2. KIRCHHOFF MIGRATION AND MODELING IN THE TIME-DOMAIN

which is an explicit form of the Kirchhoff forward modeling. In the matrix/operator notation this equation can be stated by

$$\mathbf{d} = \mathbf{L}\mathbf{m}, \quad (2.18)$$

where \mathbf{d} , \mathbf{L} , and \mathbf{m} are data, forward modeling operator, and reflectivity model, respectively.

Seismic migration may be defined as the adjoint (conjugate transpose) of the seismic modeling operator (Claerbout, 2004). The adjoint operator is only an approximation to the inverse of the forward modeling operator. The migration operator may be modified to better approximate the inverse of the forward modeling operator. Examples of the latter are given by Bleistein et al. (1987) and Jin et al. (1992) who provided high frequency asymptotic migration/inversion formulas under the assumption of infinite recording aperture.

Using matrix notation, Kirchhoff migration can be written as (Nemeth et al., 1999):

$$\hat{\mathbf{m}} = \mathbf{L}'\mathbf{d}. \quad (2.19)$$

In equation (2.19) $\hat{\mathbf{m}}$ and \mathbf{d} are the migrated model and data respectively and \mathbf{L}' is the migration operator.

Similar to equation (2.12) using equations (2.8) and (2.11) the Kirchhoff PSTM (equation 2.19) can be expressed by the explicit form of (Nemeth et al., 1999):

$$\hat{m}(x, z) = \int ds h_s(s) \int dr h_r(r) \times \left(\int d(x_s, x_r, t) A_{sx} A_{xr} W(t - \tau_{x_s, 0, x, z} - \tau_{x, z, x_r, 0}) dt \right), \quad (2.20)$$

in the time-domain, where $h_s(s)$ and $h_r(r)$ are source and receiver sampling functions respectively, d is recorded data, and \hat{m} is the migration image.

In practice, in order to implement equation (2.20), the integration is replaced by a summation and the infinite limits in the integrals are replaced by finite limits of sources

2.2. KIRCHHOFF MIGRATION AND MODELING IN THE TIME-DOMAIN

and receivers. Migration is the result of summation of all amplitudes on the data along the traveltimes hyperbola and mapping the result to an image point x, z .

This summation is called “*diffraction summation*”. Repeating the diffraction summation for each point in the image returns the earth’s reflectivity model.

In the case of time migration equations (2.15) and (2.16) are used to calculate corresponding traveltimes. Then the time τ , will be:

$$\tau = \tau_{x_s,0,x,z} + \tau_{x,z,x_r,0} = \sqrt{\frac{(x_s - x)^2}{V^2} + \frac{z^2}{V^2}} + \sqrt{\frac{(x_r - x)^2}{V^2} + \frac{z^2}{V^2}}, \quad (2.21)$$

which is called Double-Square-Root (DSR) equation.

If in equation (2.21), term z^2/V^2 replaced by $t_0/2$, half of zero-offset two-way travel-time, the DSR equation will have the following form which is used in the Kirchhoff time migration:

$$\tau = \sqrt{\frac{(x_s - x)^2}{V^2} + \frac{t_0^2}{4}} + \sqrt{\frac{(x_r - x)^2}{V^2} + \frac{t_0^2}{4}}. \quad (2.22)$$

With this parameterization our output image is given in x, t_0 (lateral position - migration time) as opposed as x, z (lateral position depth). The advantage of working in time is that we remove the complexity of computing travel-times via ray tracing by approximating reflected energy via waveform with hyperbolic travel-time signatures.

When the difference between minimum and maximum offset is large enough, it is possible to separate data to different offset bins and migrate the data of each bin separately.

The advantage of splitting the data and the migration image to different offset bins is that it keeps the offset dependent information. AVO analysis is an example of this kind of information. The migrated image can have an additional dimension, the offset, and the reflectivity can be expressed as: $m(x, z, h_i), i = 1, nh$. Also by performing migration on each offset bin separately, it is possible to have some controls or constraints on the Common Image Gather (CIG)s in LSM, as will be shown in the next chapters. CIG is a gather containing traces with same x and different offsets, $m(x = const., z, h)_{i=1, nh}$ (Section 4.2.1).

2.2. KIRCHHOFF MIGRATION AND MODELING IN THE TIME-DOMAIN

In case of considering different offsets, the Kirchhoff seismic modeling (equation 2.12) is replaced by:

$$d(x_s, x_r, t, h_i) = \int m(x, z, h_i) W(t) * G(x_r, 0, t|x, z) * \ddot{G}(x, z, t|x_s, 0) dx dz, \quad (2.23)$$
$$i = 1, nh,$$

where h_i and nh are the offset bin number and the total number of offset bins, respectively.

However, separating data to a large number of offsets needs more memory for storing copies of model. Another thing that must be considered is that the number of offsets must be chosen in a way that there are enough traces for each bin to construct an acceptable common offset image, $m(x, z, h_i)$. Experiences show with the data including hundreds of shotgathers, having 3 to 5 traces per offset bin per shot is necessary.

2.2.1 Forward and adjoint operators in midpoint offset space

A change of coordinate systems permits one to represent seismic data in midpoint-offset space:

$$x = (x_r + x_s)/2, \quad \text{midpoint,}$$

and

$$h = (x_s - x_r)/2, \quad \text{offset.}$$

Using the aforementioned change of variables the forward and adjoint operators can be expressed as a function of midpoint-offset-time (data) and midpoint-offset-migration time (reflectivity model). In our numerical implementation the operator L' maps data $d(m, h, t)$ to a subsurface model $m(x, h, t_0)$ where now the image of the reflectivity has redundancy due to the fact that the offset variable has not been removed. The subsurface image (structural image) is computed via $\sum_h m(x, h, t_0)$.

2.3 Implementation of Kirchhoff time migration/modeling

2.3.1 Migration weight

The final goal of seismic prospecting is the estimation of material properties or quantities that can be easily related to material properties. In other words, one is not only concerned with positioning layers in the subsurface but also having a quantitative assessment of the properties of the formations originating at an interface. The problem of locating layers is often called the structural imaging problem. In this case imaging is used to estimate the boundaries of the geological interfaces.

Amplitude preserving migration attempts to provide an image where the "strength of the migrated image" is proportional the true strength of the earth reflectivity. In other words we want not only to know where are the layers but how "strong" is a given interface.

Migration methods that accurately handle amplitude information are often denoted as true amplitude migration methods. True amplitude migration is achieved by including wave-theoretical weights to the diffraction summation. In other ways, weights derived from simple models are used to perform the migration in a way the recovered strength of a reflector is proportional to its true strength (or reflectivity) (Zhang et al., 2000).

Computing the weight function in Kirchhoff migration is done in the most internal loop of the algorithm. The latter will notably increases the cost of migration. Therefore approximate weights with a function which can be computed outside the internal loops reduces the migration cost.

However, for many purposes the following simplified weight function satisfies both weight and obliquity factor and is used in the industry:

$$Wg = \left(\frac{t_0}{\tau} \right). \quad (2.24)$$

where t_0 is zero-offset traveltime and τ is migration time.

2.3.2 Migration aperture

Kirchhoff migration is a costly procedure in the seismic data processing flow. The cost grows higher when an iterative method (for example CG) is used similar to the method

2.3. IMPLEMENTATION OF KIRCHHOFF TIME MIGRATION/MODELING

of LS-PSTM. Each sample in the output image is a result of summation of all amplitudes along the hyperbola's flank, multiplied by the corresponding calculated weight factor.

The amplitude terms are small and negligible for image points far from the trace position. Restricting the summation to a certain distance from the trace position reduces the cost of migration without significant changing the result. This restriction is called the *migration aperture* implementation.

Because steeper dips are excluded when the aperture is small, a small aperture will also help to avoid spatial aliasing (Abma et al., 1999). Small aperture also increases the S/N ratio by reducing the stacking of noises far from image point (Hertweck et al., 2003). Kirchhoff migration is limited to the area of seismic data acquisition, therefore it automatically has an aperture limitation. However, the limitation imposed by the cable length may not be sufficient and one needs to impose an extra limitation onto the algorithm.

It is important to stress that a small aperture might not preserve amplitudes since one is ignoring the effect of events far from the image point. Therefore a large enough aperture is required to preserve amplitudes in the migrated image. In addition, a narrow aperture will filter out necessary dipping events and smears the data in the deeper part of the migrated image (Rastogi and Phadke, 2002). In short, as often in geophysics, there is a trade-off at the time of selecting the aperture for our algorithm. In this thesis I propose to use a time-variant aperture by increasing width of aperture while increasing time (or depth). This is illustrated in Figure (2.1 b). Choosing the right aperture size is an important decision in Kirchhoff migration since it affects both the quality and cost of algorithm.

Using a dynamic ray tracing method, Schleicher et al. (1997) showed that the minimum migration aperture can be calculated from the projected Fresnel zone for a certain frequency. In the case of linear events, when the aperture is larger than twice the Fresnel zone size, the migration amplitudes are true reflection amplitudes (Sun and Bancroft, 2001). The Fresnel zone is the circle area on the reflector where a spherical wave sweeps after first touch, during half wavelength penetration. This area is shown schematically by $m1m2$ in Figure (2.2). For a wave with single frequency f in a zero-offset section, the Fresnel zone radius is equal to (Sheriff, 1980)

2.3. IMPLEMENTATION OF KIRCHHOFF TIME MIGRATION/MODELING

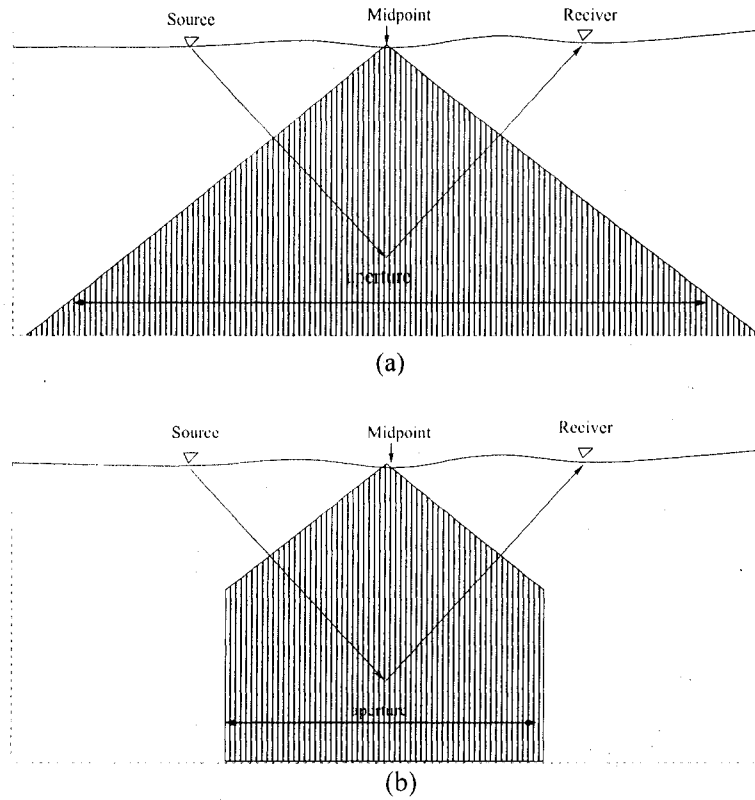


Figure 2.1: Implementation of aperture in Kirchhoff PSTM. a) A triangular aperture. b) A combination of triangle and constant aperture. For each trace in the midpoint position, Kirchhoff summation is applied on samples in the area inside the aperture.

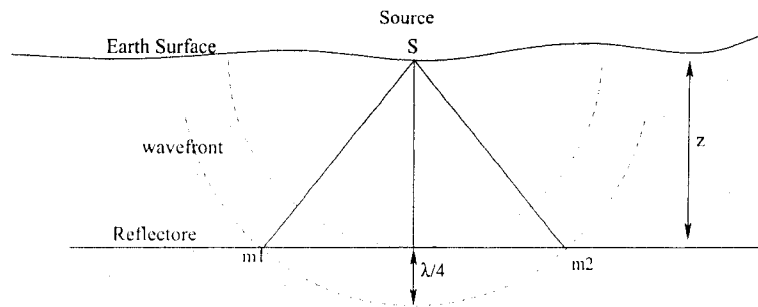


Figure 2.2: Fresnel zone for a wave with wavelength = λ is equal to the distance of m_1m_2 .

$$R_{f_{h0}} = \frac{V_{RMS}}{2} \sqrt{\frac{t_0}{f}}, \quad (2.25)$$

2.3. IMPLEMENTATION OF KIRCHHOFF TIME MIGRATION/MODELING

where t_0 is zero-offset two-way traveltimes and V_{RMS} is RMS velocity. To derive the size of prestack Fresnel zone as a function of offset for an offset sections, we consider the double-square-root (DSR) equation for Kirchhoff traveltimes calculation in an offset section:

$$t_k = \sqrt{\frac{t_0^2}{4} + \frac{(x+h)^2}{V^2}} + \sqrt{\frac{t_0^2}{4} + \frac{(x-h)^2}{V^2}}, \quad (2.26)$$

here h is half-offset, x is the horizontal distance between the midpoint and the scatterer point.

By calculating the square of t_k , the DSR equation (2.26) has the following form:

$$t_k^2 = \frac{t_0^2}{2} + \frac{2(x^2 + h^2)}{V^2} + \sqrt{\frac{t_0^4}{4} + \frac{2(x^2 + h^2)}{V^2}t_0^2 + 4\frac{(x^2 - h^2)^2}{V^4}}, \quad (2.27)$$

which can be rewritten as:

$$t_k^2 = \frac{t_0^2}{2} + \frac{2(x^2 + h^2)}{V^2} + \sqrt{\frac{t_0^4}{4} + \frac{2(x^2 + h^2)}{V^2}t_0^2 + 4\frac{(x^2 + h^2)^2}{V^4} - \frac{16x^2h^2}{V^4}}, \quad (2.28)$$

After defining the following new variable:

$$a = \frac{t_0^2}{2} + \frac{2(x^2 + h^2)}{V^2}, \quad (2.29)$$

Equation (2.28) can be expressed by:

$$t_k^2 = a + \sqrt{a^2 - \frac{16x^2h^2}{V^4}}. \quad (2.30)$$

2.3. IMPLEMENTATION OF KIRCHHOFF TIME MIGRATION/MODELING

By calculating the square of t_k^2 , we have:

$$t_k^4 = 2a^2 - \frac{16x^2h^2}{V^4} + 2a\sqrt{a^2 - \frac{16x^2h^2}{V^4}} = 2a^2 - \frac{16x^2h^2}{V^4} + 2a(t_k^2 - a), \quad (2.31)$$

or

$$t_k^4 = 2at_k^2 - \frac{16x^2h^2}{V^4}, \quad (2.32)$$

By some mathematical computation and substituting a from equation (2.29) the DSR equation can be exactly expressed by (Sun and Bancroft, 2001):

$$t_k^2 = t_0^2 + \frac{4\left(x^2 + h^2 - \frac{4x^2h^2}{V^2t_k^2}\right)}{V^2}. \quad (2.33)$$

If we consider x as the Fresnel zone radius displacement, R_{f_h} , then t_k will be replaced by $t_h + T/2$ where $T = 1/f$ is the period of the source wavelet and $t_h = \sqrt{t_0^2 + 4h^2/V^2}$, is the migration traveltime for offset, $2h$, as seen in Figure (2.3) (Sun and Bancroft, 2001):

$$\left(\sqrt{t_0^2 + \frac{4h^2}{V^2}} + \frac{T}{2}\right)^2 = t_0^2 + \frac{4\left(R_{f_h}^2 + h^2 - \frac{4R_{f_h}^2h^2}{V^2t_h^2}\right)}{V^2}. \quad (2.34)$$

The Fresnel zone radius for an offset section, R_{f_h} , can be exactly expressed by (Sun and Bancroft, 2001):

$$R_{f_h} = \sqrt{\frac{TV^2\sqrt{t_0^2 + \frac{4h^2}{V^2}}}{4 - \frac{16h^2}{V^2t_0^2 + 4h^2}}}. \quad (2.35)$$

The best minimum aperture for each depth (time) is twice of the Fresnel zone diameter at that depth (time). This minimum aperture size has a direct relationship with depth

2.3. IMPLEMENTATION OF KIRCHHOFF TIME MIGRATION/MODELING

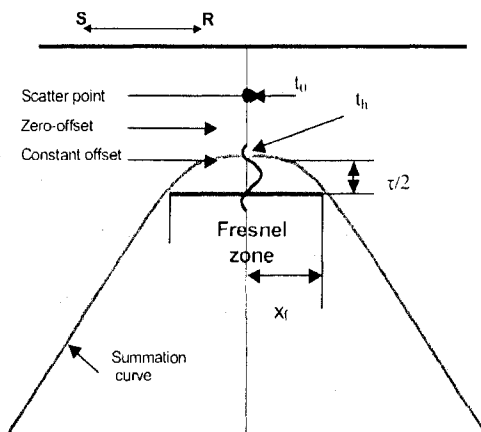


Figure 2.3: Fresnel zone for an offset section after Sun and Bancroft (2001). Here, x_f is Fresnel zone radius and t_h is the offset traveltime h is half source-receiver distance.

(time). Calculating equation (2.35) “on the fly” for each depth (time) increases the cost of migration. It is better to start the aperture at surface with a triangle and continue it to reach the width of a pre-calculated minimum aperture for all depths (times) as a constant aperture until the end of the section.

2.3.3 Spatial anti-aliasing of the migration operator

Migration operator aliasing is different from data aliasing or image aliasing. According to sampling theory, if there are frequencies in the seismic data greater than f_d given by

$$f_d = V_r / (4 \sin \theta_r \Delta p), \quad (2.36)$$

for a local plane wave with the incident angle of θ_r with the recording surface, data aliasing occurs (Lumley et al., 1994). In equation (2.36) Δp is the trace spacing, and V_r is the velocity at the receiver location. After recording aliased data, it is difficult to remove the aliasing artifacts. To avoid data aliasing, the receiver spacing must be chosen small enough during data acquisition. In data processing, one way to overcome spatial aliasing is to reduce the trace spacing (Δp in equation (2.36)) by adding interpolated traces (without interpolating the aliased events) between existing traces. On the other hand, image aliasing simply can be avoided just by building a finer grid in the image space.

2.3. IMPLEMENTATION OF KIRCHHOFF TIME MIGRATION/MODELING

As shown by Lumley et al. (1994) and Bevc and Lumley (1994), Kirchhoff migration operator aliasing exists for all frequencies above f_{max} , where

$$f_{max} = \frac{1}{2 \left(\frac{\partial t_k}{\partial \rho} \right) \Delta p}, \quad (2.37)$$

and $(\partial t_k / \partial \rho) \Delta p$ is the time shifting operator between two adjacent traces and Δp is equal to trace spacing in 2D and $\sqrt{(\Delta x \cos \theta)^2 + (\Delta y \sin \theta)^2}$ in case of the 3D, where Δx and Δy are in- and cross-line trace spacing, respectively. The highest frequency in the data is (Bevc and Lumley, 1994)

$$f_d = \frac{1}{2P\Delta p}, \quad (2.38)$$

where $P = \delta t / \delta x$ is the maximum stepout or dip in the events. It means that with a trace spacing of Δp and P as a stepout of the layer, f_d is the maximum frequency in data that we can have without aliasing.

The anti-aliasing is necessary when the frequency content of data lies between f_d and f_{max} . A 3D data acquisition is relatively expensive and the acquired data is irregular and sparse. Therefore, usually anti-aliasing is more necessary in 3D Kirchhoff migration than in 2D implementations. Aliasing in the migration operator produces migration noise. The migration noise may be seen in the migrated seismic section as artifacts (Abma et al., 1999).

The simplest way to avoid aliasing in the Kirchhoff migration is truncating migration operator by aperture limitation and operator dip filtering. Another possibility is decreasing the distance between traces by adding some new interpolated traces as we do in data antialiasing. Gray (1992)'s method for avoiding aliasing in the Kirchhoff migration operator includes low-pass filtering the input traces. But this method increases the data volume and consequently the migration cost, by several times copying the input data and low-pass filtering them with different high-cut frequencies. The latter is not viable for LS-PSTM where all the data volume is kept in memory during the optimization process (this is discussed in Chapter 4).

The method given by Claerbout (1992) and Lumley et al. (1994) is the most convenient for our algorithm. In Lumley et al.'s (1994) method, the maximum un-aliased frequency of the operator at each point is calculated, then a triangle filter is designed to remove

2.3. IMPLEMENTATION OF KIRCHHOFF TIME MIGRATION/MODELING

the higher frequencies in the data by a smoothing operator. They reduced the N -point triangle filter to one three-point operator. This operator is a result of summation of three (shifted and/or scaled) ramp functions $r(n+k-1)$, $2r(n)$ and $-r(n-k-1)$ where k is shifting amount. The operator $r(n)$ and its Z transform are given by:

$$r(n) = \begin{cases} n & n \geq 0 \\ 0 & n \leq 0 \end{cases} \iff r(z) = \frac{z^{-1}}{(1-z^{-1})^2} \quad (2.39)$$

The summation in the Z domain is (Lumley et al., 1994)

$$g(z) = \frac{-z^{-k-1} + 2z - z^{k+1}}{\alpha(1-z)(1-z^{-1})}, \quad (2.40)$$

where $\alpha = (k+1)^2$.

By replacing z by $e^{-i\omega\Delta t}$ the amplitude spectrum of $g(z)$ is obtained (Lumley et al., 1994):

$$A(\omega) = \frac{\sin^2(\omega\Delta t(k+1)/2)}{\sin^2(\omega\Delta t/2)}, \quad (2.41)$$

which is discrete version of sinc^2 function. Hence, $g(z)$ is the Z transform of a triangular smoothing operator of length $N = 2k + 1$. When we want f_{max} as the maximum non-aliased frequency, we choose N in such a way that the first notch of the sinc^2 function attenuates f_{max} . Therefore

$$N \geq \frac{2}{\Delta t f_{max}}, \quad (2.42)$$

satisfies operator anti-aliasing.

As mentioned by Lumley et al. (1994), the denominator of $g(z)$ is composed of a causal integration of the trace ($1/(1-z)$) followed by an anticausal integration of the trace ($1/(1-z^{-1})$). The nominator is a gaped three-point Laplacian operator where the length of gap determines f_{max} .

Lumely's anti-aliasing operator is less expensive than other methods, however, triangle smoothing is not a perfect method of filtering due to excessive ringing. Despite the efficiency of the three-point operator it also adds some extra expense to the migration operator. As argued by Abma et al. (1999), the two summations along the seismic trace also

2.3. IMPLEMENTATION OF KIRCHHOFF TIME MIGRATION/MODELING

may cause some numerical precision problems. However, it is better to implement it only when it is necessary to control the aliasing operator by limiting the migration aperture. With small enough migration aperture and in areas with attenuation of high frequencies, anti-aliasing might be unnecessary.

2.3.4 Pseudocode for Kirchhoff time migration/modeling

Claerbout and Black (2005) 's simple tutorial code for migration and modeling is a good reference for understanding the necessary concepts of migration and modeling algorithms. Based on their code we provided a functional code in Fortran which considers more practical aspects of migration.

In this code we consider the Kirchhoff PSTM as adjoint and the Kirchhoff forward modeling as forward. We added interpolation and antialiasing by Lumley et al. (1994)'s method in the adjoint and also in the modeling. Aperture implementation, a proper weight function, and cross correlation and convolution with the wavelet in the case of adjoint and forward are considered. The ability to do migration and modeling in different offset domains and also parallel coding with OpenMP (Chandra et al., 2001) in order to accelerate running the code using multiprocessor computers are other additions to the code.

In this code, $M(\tau, x, h)$ is the model matrix where x is horizontal distance vector, τ is two way time, and h is offset and D is data matrix. Also, $V(\tau, x)$ represents the RMS velocity in the image position.

Pseudocode for Kirchhoff time migration/modeling:

```
if adjoint == true
```

```
     $M(\tau, x, h) = 0$ 
```

```
Endif
```

```
If forward == true
```

```
     $D(nt, ntrace) = 0$ 
```

```
Endif
```

2.3. IMPLEMENTATION OF KIRCHHOFF TIME MIGRATION/MODELING

Start parallelization (OpenMP)

Do $k = 1, ntrace$

If *adjoint* == *true*

X-correlation of trace with wavelet

Double integration of trace

Endif

Calculate offset index, *nh*, for the trace

Do $i\tau = 1, n\tau$

Calculate aperture indexes: *ixmin*, *ixmax*

Do $ix = ixmin, ixmax$

$$t = \left(\left(\frac{x(ix) - r(k)}{V(i\tau, ix)} \right)^2 + \left(\frac{\tau(i\tau)}{2} \right)^2 \right)^{0.5} + \left(\left(\frac{x(ix) - s(k)}{V(i\tau, ix)} \right)^2 + \left(\frac{\tau(i\tau)}{2} \right)^2 \right)^{0.5}$$

$it = t/dt$

$dtt = 1 - 100(t - it \cdot dt)$

Calculate length the antialiasing filter= N

Calculate weight= Wg

If $it < nt - N$ and $it > N$

If *forward* == *true*

$trace(it) = trace(it) + M(i\tau, ix, nh) * dtt * Wg$

$trace(it + 1) = trace(it + 1) + M(i\tau, ix, nh) * (1 - dtt) * Wg$

$trace(it - N) = trace(it - N) - 0.5 * M(i\tau, ix, nh) * dtt * Wg$

$trace(it - N + 1) = trace(it - N + 1) - 0.5 * M(i\tau, ix, nh) * (1 - dtt) * Wg$

$trace(it + N) = trace(it + N) - 0.5 * M(i\tau, ix, nh) * dtt * Wg$

$$\text{trace}(it + N + 1) = \text{trace}(it + N + 1) - 0.5 * M(i\tau, ix, nh) * (1. - dtt) * Wg$$

Endif

If adjoint == true

$$\begin{aligned} M(i\tau, ix, nh) = & M(i\tau, ix, nh) + (\text{trace}(it) - 0.5 * (\text{trace}(it - N) \\ & + \text{trace}(it + N))) * dtt * Wg + (\text{trace}(it + 1) - 0.5 * \\ & (\text{trace}(it - N + 1) + \text{trace}(it + N + 1))) * (1. - dtt) * Wg \end{aligned}$$

Endif

Endif

Enddo

Enddo

If forward == true

Double integration of trace

Convolution of trace with wavelet

Endif

Enddo

End parallelization

2.4 Summary

In this chapter, a formulation of migration/de-migration in terms of Kirchhoff diffraction integrals was provided.

The migration aperture and antialiasing operator were defined as well. Also the basic equations for the PreStack Kirchhoff time modeling as the adjoint of Kirchhoff PSTM were presented.

We finally provide an algorithm to construct the two canonical operators needed by this thesis: the forward modeling operator and its adjoint also called the migration operator.

Chapter 3

Seismic Data Migration and Inversion

3.1 Discrete inverse theory

As defined by Menke (1989), inverse theory is a set of computational methods used to reduce geophysical data to information about the physical world. Discrete inverse theory uses matrix equations rather than integrals which are often used in the continuous formulation of inverse theory. The solution to an inverse problem is often found by minimizing the difference between the real observations and synthetic data computed via forward modeling.

Most geophysical problems are ill-posed. In other words, problems that do not have a unique and stable solution. Ill-posed problems are neither completely under-determined nor completely over-determined. We often acquire more observations than unknown model parameters. The observations, however, are often not linearly independent. To retrieve a unique, stable solution, the cost function is modified by the addition of a regularization term or other constraint.

In this chapter we study the linear inverse problem associated to the inversion of the Kirchhoff de-migration operator. In other words, the data are assumed to be generated by a de-migration operator acting on a reflectivity model. The goal is to retrieve the reflectivity in the presence of noise and incompleteness of the recorded wave field.

3.2 Kirchhoff LS-PSTM

Many seismic processing and imaging problems can be written in the general form of

$$\mathbf{d} = \mathbf{L}\mathbf{m} + \mathbf{n}. \quad (3.1)$$

where \mathbf{d} is the data, \mathbf{m} is the model and \mathbf{L} is an operator acting on \mathbf{m} . Radon Transforms and deconvolution are two examples that can be formulated as a linear inverse problems. We have also included a modeling error or noise term denoted by \mathbf{n} . Seismic modeling or de-migration is another example of an operator that can be written in terms of a linear model as shown in Chapter 2. This is valid in the linear imaging method where one assumes a known background velocity model and data composed of primary reflections. In that case one attempts to invert for perturbations such as velocity or impedance disturbances or, like in our case, a model of the subsurface reflectivity (deBruin et al., 1990).

An imaging problem is the solution of the inverse problem where from incomplete and inaccurate data \mathbf{d} , one attempts to retrieve a model of the subsurface \mathbf{m} . Without going into much detail, the model of the subsurface can be given by actual physical parameter perturbations or by signals easily related to the model parameter perturbations. An example of the latter are angle and offset gathers (Lumley and Beydoun (1997), Bleistein (2002), Kuehl and Sacchi (2003) and Wang and Sacchi (2007)). In this case one can find the solution \mathbf{m} by solving an inverse problem. We attempt to extract the important subsurface information via an optimization problem where one needs to minimize the following cost function:

$$J(\mathbf{m}) = \|\mathbf{L}\mathbf{m} - \mathbf{d}\|^2 + \mu^2 \mathcal{R}(\mathbf{m}). \quad (3.2)$$

The cost function J is composed of two terms. The first term is the data misfit. The latter term stresses the fact that the recovered image of the subsurface must honor the observations. We are also making the usual assumption of normally distributed errors. This assumption leads to the l_2 -norm misfit measure (Beydoun and Mendes, 1989). The second part of the cost function, $\mathcal{R}(\mathbf{m})$, is called the regularization term. It is a penalty term that serves to eliminate models with undesired features, for instance, models with

non-smooth character along one or more spatial dimensions. The trade-off parameter μ is used to balance the amount of regularization versus the amount of misfit reduction. The trade-off parameter permits one to produce a family of solutions with different level of data fitting. If the parameter μ is small, the regularization term becomes negligible and the focus is on the reduction of the misfit. The latter is quite dangerous; one can produce solutions where data overfitting translates in unstable models. On the other hand, if μ is a large number, the regularization term dictates the form of the solution and the data is underfit. In other words, the model of the subsurface does not honor the observations.

Nemeth et al. (1999) showed that one can represent pre-processed seismic data \mathbf{d} as follows:

$$\mathbf{d} = \mathbf{L}\mathbf{m} + \mathbf{n} \quad (3.3)$$

where \mathbf{m} , \mathbf{L} and \mathbf{n} are the real reflectivity model vector, forward modeling operator and noise, respectively. For simplicity if we assume that $\mathbf{n} \simeq \mathbf{0}$ then by substituting equation (2.18) into (2.19) we have:

$$\hat{\mathbf{m}} = \mathbf{L}'\mathbf{L}\mathbf{m}. \quad (3.4)$$

If \mathbf{L} is the Kirchhoff de-migration operator, then \mathbf{L}' is the transpose or adjoint operator. The transpose operator \mathbf{L}' maps data to model space (migration). The latter shows that Kirchhoff migration will reconstruct the real earth model \mathbf{m} if the operator $\mathbf{L}'\mathbf{L}$ is an identity matrix. This is only true if \mathbf{L} is an orthogonal operator. However, $\mathbf{L}'\mathbf{L}$ is not an identity matrix. It has off-diagonal non-zero elements (Nemeth et al., 1999). The departure of $\mathbf{L}'\mathbf{L}$ from the identity matrix is due to geometrical spreading losses, incompleteness or irregularity in the data sampling and illumination problems associated to sparse ray coverage (Nemeth et al., 1999).

We first consider the minimization of the cost function, J , by setting the regularization term equal to zero ($\mu = 0$). We take derivatives of the cost function with respect to model parameters and set them to zero and arrive to the classical least-squares solution:

$$\hat{\mathbf{m}} = (\mathbf{L}'\mathbf{L})^{-1}\mathbf{L}'\mathbf{d}. \quad (3.5)$$

The last equation serves to illustrate a couple of interesting points. First, it is clear that the migrated image expressed as $\mathbf{L}'\mathbf{d}$ is corrected (de-blurred) by the inverse operator $(\mathbf{L}'\mathbf{L})^{-1}$ to produce the inverted image. From this point of view least-squares migration can be considered similar to classical migration with an adjoint operator modified via a de-blurring operator. Secondly, one needs to realize that in practice it is not possible to calculate $(\mathbf{L}'\mathbf{L})^{-1}$ because either it is non-invertible or large. Therefore, finding an approximate of \mathbf{m} by an iterative method like Conjugate Gradients (CG) is recommended. The advantage of this method is that we do not need to have the matrices \mathbf{L} and \mathbf{L}' . We can use the forward and adjoint subroutines instead. In scenes rather than computing the solution via direct inversion of the operator $\mathbf{L}'\mathbf{L}$, the method of CG minimizes the cost function by a series of steps (iterations).

An important aspect of working with the method of CG is that the number of iterations can be truncated to obtain an approximate solution to our optimization problem. In general, an approximate solution is desirable as we often want to reduce computational time and avoid overfitting the data.

3.3 Regularized Kirchhoff LS-PSTM

As Nemeth et al. (1999) showed, migration artifacts can be attenuated by minimizing the general objective function of the form:

$$J(\mathbf{m}) = \|\mathbf{L}\mathbf{m} - \mathbf{d}\|^2 + \mu^2 \mathcal{R}(\mathbf{m}). \quad (3.6)$$

In equation (3.6), \mathcal{R} is the regularization function which is often chosen according to a priori information about the unknown model \mathbf{m} . An example is the similarity of adjacent common offset images used by Duquet et al. (2000). As we have already mentioned, the trade-off parameter μ controls the amount of regularization. A small μ gives more weight for minimizing the misfit over the model norm and vice versa. To minimize the objective function (3.6) we must take its derivatives with respect to \mathbf{m} and set them to zero

$$\frac{dJ(\mathbf{m})}{d\mathbf{m}} = 0. \quad (3.7)$$

3.3. REGULARIZED KIRCHHOFF LS-PSTM

The regularization function \mathcal{R} can be chosen from a variety of functions (Sacchi et al., 2006):

1. If $\mathcal{R}(\mathbf{m}) = \|\mathbf{m}\|_2^2$, which is the Euclidean norm of the model, the solution is called the "minimum norm solution" or "Damped Least-Squares" or the "Least-squares solution with zero-order quadratic regularization" (Tikhonov, 1963).

The solution is given by:

$$\mathbf{m} = (\mathbf{L}'\mathbf{L} + \mu^2\mathbf{I})^{-1}\mathbf{L}'\mathbf{d}. \quad (3.8)$$

2. If $\mathcal{R}(\mathbf{m}) = \|\mathbf{D}_{1h_x}\mathbf{m}\|_2^2$ and \mathbf{D}_{1h_x} is the first order derivative in the offset direction:

$$\mathbf{D}_{1h_x} = \begin{pmatrix} -1 & 1 & 0 & 0 \\ 0 & -1 & 1 & 0 \\ 0 & 0 & -1 & 1 \\ 0 & 0 & 0 & -1 \end{pmatrix}. \quad (3.9)$$

The derivative is a high-pass filter, therefore minimizing a cost function with this regularization function is equivalent to penalizing high frequency solutions. Higher order of derivatives are possible as well. For instance we may replace \mathbf{D}_{1h_x} by \mathbf{D}_{2h_x} where

$$\mathbf{D}_{2h_x} = \begin{pmatrix} 1 & -2 & 1 & 0 \\ 0 & 1 & -2 & 1 \\ 0 & 0 & 1 & -2 \\ 0 & 0 & 0 & 1 \end{pmatrix}. \quad (3.10)$$

Using first and second order derivative operators leads to the following solutions

$$\mathbf{m} = (\mathbf{L}'\mathbf{L} + \mu^2\mathbf{D}'_{1h_x}\mathbf{D}_{1h_x})^{-1}\mathbf{L}'\mathbf{d}. \quad (3.11)$$

and

$$\mathbf{m} = (\mathbf{L}'\mathbf{L} + \mu^2 \mathbf{D}'_{2h_x} \mathbf{D}_{2h_x})^{-1} \mathbf{L}'\mathbf{d}, \quad (3.12)$$

respectively.

3. If we chose $\mathcal{R}(\mathbf{m}) = \sum_{i=1}^M |m_i|$ we have an l_1 norm regularization. Minimizing an objective function with this regularization produces sparse solutions. The l_1 norm solution has this form (Wang, 2005):

$$\mathbf{m} = (\mathbf{L}'\mathbf{L} + \mu^2 \mathbf{Q}(\mathbf{m}))^{-1} \mathbf{L}'\mathbf{d} \quad (3.13)$$

where \mathbf{Q} is a diagonal matrix with the diagonal elements:

$$Q_{ii} = \begin{cases} |m_i|^{-1} & \text{if } |m_i| > \epsilon \\ \epsilon^{-1} & \text{if } |m_i| < \epsilon \end{cases}$$

and ϵ is a threshold value.

It is clear that the l_1 solution requires an iterative algorithm as \mathbf{Q} depends on unknown model parameters.

3.3.1 The Method of Conjugate Gradients (CG)

The operator $\mathbf{L}'\mathbf{L}$ can be inverted via direct solvers whenever \mathbf{L} is not a large operator. In general, the dimensions of \mathbf{L} are number of observations \times number of cells used to describe the subsurface model. In a typical seismic survey the number of observations can be of the order of 10^7 and the number of cells (for a 3D survey) of the order of 10^5 . It is clear, that in real scenarios \mathbf{L} is a large operator not amenable of direct manipulations.

For small problems, one could use a direct method. In this case the solution can be found by calculating the inverse of the matrix $\mathbf{L}'\mathbf{L}$ by a conventional method such as Gaussian elimination (Strang, 1986). In reality, not only \mathbf{L} is a large operator but in addition, it does not have an explicit matrix form. In other words, we never have access to \mathbf{L} in the form of a matrix. The operator \mathbf{L} is a function (subroutine) that given an input vector (\mathbf{m}) produces an output vector of observations \mathbf{d} . Similarly, the transpose

(adjoint) operator L' is a function (subroutine) that takes an input d to produce an output vector m' (a vector that belongs to the space of models). To summarize, we do not have matrices, we do have operators and therefore we need to use an iterative strategy that relies of the action of L and L' on model and data space vectors, respectively.

With the previous discussion in mind, the cost function can be minimized using two algorithms. One possibility is to use the Steepest Descent method where we need to assume that $L'L$ is positive definite. With this condition, the cost function is a paraboloid with a single minimum at the solution point. The algorithm follows the opposite direction of the largest gradient until it reaches a minimum. Then it changes the direction and follows a new descent direction. The problem with this method is that the algorithm requires too many steps to find the right path toward the minimum (Strang, 1986). A more efficient alternative is to use the method of Conjugate Gradients (CG). The CG algorithm is able to follow directions orthogonal to all previous steps. Subsequently it finds the minimum more quickly than the Steepest Descent method.

The method of CG initially introduced by Hestenes and Steifel (1952) is used solve a system of linear equation of the form

$$Ax = b \tag{3.14}$$

where A is a positive-definite symmetric matrix and b and x are data and unknown vectors, respectively. In our case, it can be used to solve the problem

$$L'Lm = L'd \tag{3.15}$$

where $L'L$ is symmetric as required by the CG method. A modified version of the CG method (Scales, 1987), known as least-squares conjugate gradients (LSCG), works directly with the operators L and L' and does not require the new operator $L'L$ to be found. The CGLS method is summarized as follows:

Initialization

$$m_0 = 0$$

$$s_0 = d - Lm_0 = d$$

$$\begin{aligned}
 \mathbf{r}_0 &= \mathbf{L}'\mathbf{s}_0 && \boxed{\text{Migration}} \\
 \mathbf{p}_0 &= \mathbf{r}_0 \\
 \mathbf{q}_0 &= \mathbf{L}\mathbf{p}_0 && \boxed{\text{Modeling or de-migration}} \\
 i &= 0
 \end{aligned}$$

Do while $i \leq \#$ of iterations

$$\begin{aligned}
 \alpha_{i+1} &= \frac{\mathbf{r}_i \cdot \mathbf{r}_i}{\mathbf{q}_i \cdot \mathbf{q}_i} \\
 \mathbf{m}_{i+1} &= \mathbf{m}_i + \alpha_{i+1}\mathbf{p}_i \\
 \mathbf{s}_{i+1} &= \mathbf{s}_i - \alpha_{i+1}\mathbf{q}_i \\
 \mathbf{r}_{i+1} &= \mathbf{L}'\mathbf{s}_{i+1} && \boxed{\text{Migration}} \\
 \beta_{i+1} &= \frac{\mathbf{r}_{i+1} \cdot \mathbf{r}_{i+1}}{\mathbf{r} \cdot \mathbf{r}} \\
 \mathbf{p}_{i+1} &= \mathbf{r} + \beta\mathbf{p}_i \\
 \mathbf{q}_{i+1} &= \mathbf{L}\mathbf{p}_{i+1} && \boxed{\text{Modeling or de-migration}} \\
 i &= i + 1
 \end{aligned}$$

EndDo

It is clear that the cost of the algorithm is dominated by the cost of applying the operator \mathbf{L} (modeling or de-migration) and \mathbf{L}' (migration) times the number of iterations.

At this point some comments are in order. In the previous analysis of CGLS we have assumed no regularization term ($\mu = 0$) and one may think that the algorithm will not converge as the operator $\mathbf{L}'\mathbf{L}$ may not be positive definite. In this situation, the CG algorithm converges to the minimum norm solution providing that the method is initialized with the null solution $\mathbf{m} = \mathbf{0}$ (Strang, 1986).

In the case of using a regularization term in the form of damping or a first/second derivative, equation (3.1) will be replaced by

$$\tilde{\mathbf{L}}\mathbf{m} = \tilde{\mathbf{d}} \tag{3.16}$$

where

$$\tilde{\mathbf{L}} = \begin{pmatrix} \mathbf{L} \\ \mu\mathbf{I} \end{pmatrix} \quad \text{for regularization with damping term,} \quad (3.17)$$

or

$$\tilde{\mathbf{L}} = \begin{pmatrix} \mathbf{L} \\ \mu\mathbf{D}_{1h_x} \end{pmatrix} \quad \text{for regularization with first order derivative,} \quad (3.18)$$

and

$$\tilde{\mathbf{d}} = \begin{pmatrix} \mathbf{d} \\ \mathbf{0} \end{pmatrix}. \quad (3.19)$$

To summarize, CG is quite flexible as it permits the incorporation of regularization terms and operates without the necessity of prescribing matrices in implicit form.

3.4 Summary

Many problems encountered in seismic data processing are ill-posed problems. As stated by the Discrete Inverse Theory, the solution to these problems can be found by minimizing the differences between the real data (observations) and the synthetic data computed using discrete operators with the addition of a regularization term to stabilize the solution.

In this chapter, I have discussed how one can pose imaging as an inverse problem. In particular, the problem of dealing with large (non-invertible operators) can be circumvented via the method of conjugate gradients. Using CG we do not need operators in explicit form, the forward and adjoint operators (de-migration and migration pair) are implemented via subroutines and never stored in memory as matrices.

Chapter 4

LS-PSTM for Resolution and Regularization of Incomplete and Irregular Data

4.1 Migration of incomplete synthetic data

Kirchhoff PSTM is commonly used for seismic imaging. The ability to work with incomplete and/or irregularly sampled data is one of the advantages of Kirchhoff PSTM. As mentioned in Chapter one, Kirchhoff PSTM can lead to accurate images of the subsurface in cases of low geological complexity.

In practice, irregularity or incompleteness of seismic data is inevitable. When data are incomplete or irregular, Kirchhoff time migration will generate seismic images dominated by artifacts. The problem is severe in 3D acquisitions. The concept, however, will be illustrated with 2D problems where the "bad" sampling was created by removing data from known data sets prior to imaging. In other words, I am trying to prove a concept and it is clear that more work is needed to extend my findings to 3D real world industrial implementations.

To show the effect of incomplete data in the migrated image, I consider an earth reflectivity model with variable background velocity. The model is portrayed in Figure (4.1). This is an earth model with a few horizontal, dipping and folded layers. All layers have undergone normal faulting. The velocity increases from $1200m/s$ at the top to $2150m/s$ at the bottom. The model is $4km$ long in the horizontal direction and 2 seconds deep vertically.

4.1. MIGRATION OF INCOMPLETE SYNTHETIC DATA

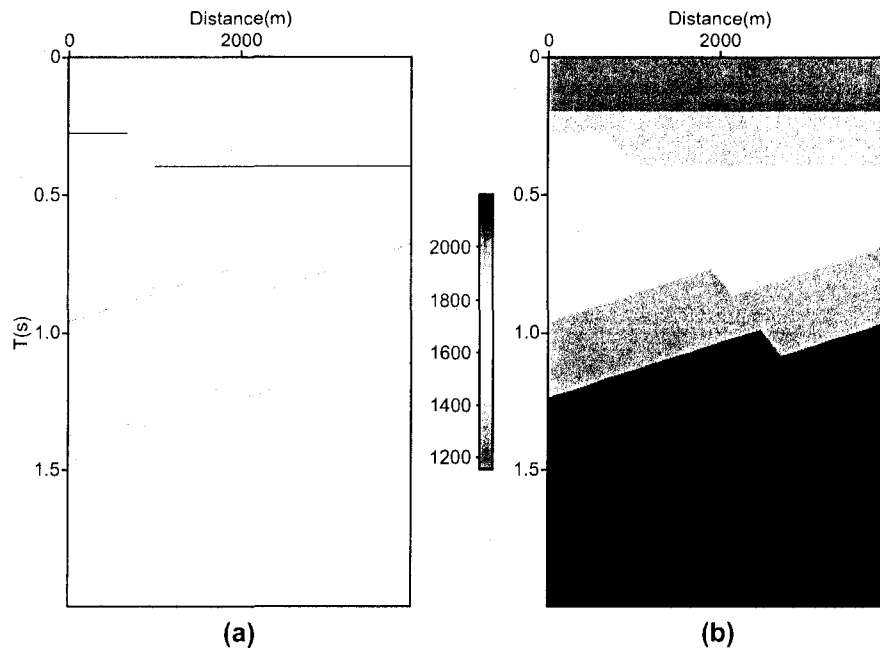


Figure 4.1: Synthetic model used to test PSTM and LS-PSTM. a) Reflectivity model. b) Velocity model. The vertical bar indicates compressional seismic velocities in m/s .

The Kirchhoff time modeling operator was adopted to generate synthetic data. A very dense acquisition pattern including 80 shots with 50m spacing and 140 receivers per shot with 10m spacing was used to illuminate the model. The time sampling interval is 4ms. A Ricker wavelet with the dominant frequency of 18Hz was used to synthesize the seismic source. In addition 5% random Gaussian noise is added to the data. Figure (4.2 a) shows a portion of a shot gather from the synthetic data set. Kirchhoff PSTM was used to estimate the image provided in Figure (4.2 b).

The effect of data irregularity is investigated by randomly removing traces from the data set. Figures (4.3)a and c show the effect of randomly removing 75% and 90% of the data, respectively. Figures (4.3)b and d portray the PSTM of the decimated data. As expected, the images are dominated by artifacts.

4.1. MIGRATION OF INCOMPLETE SYNTHETIC DATA

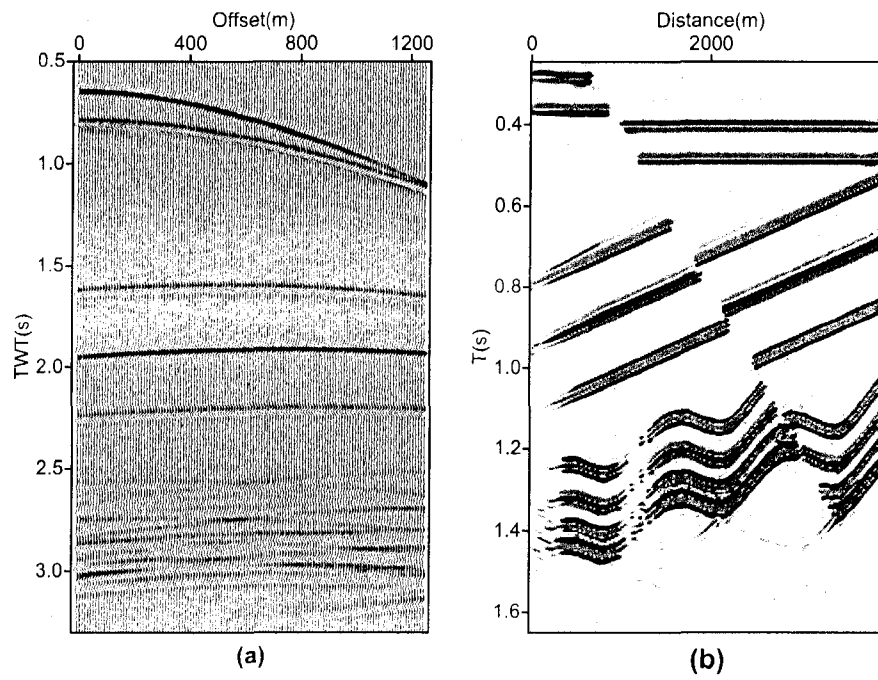


Figure 4.2: a) Synthetic data generated from the reflectivity model in in Figure (4.1) displaying 125 traces from one shot gather. b) Seismic image generated via Kirchhoff PSTM.

4.1. MIGRATION OF INCOMPLETE SYNTHETIC DATA

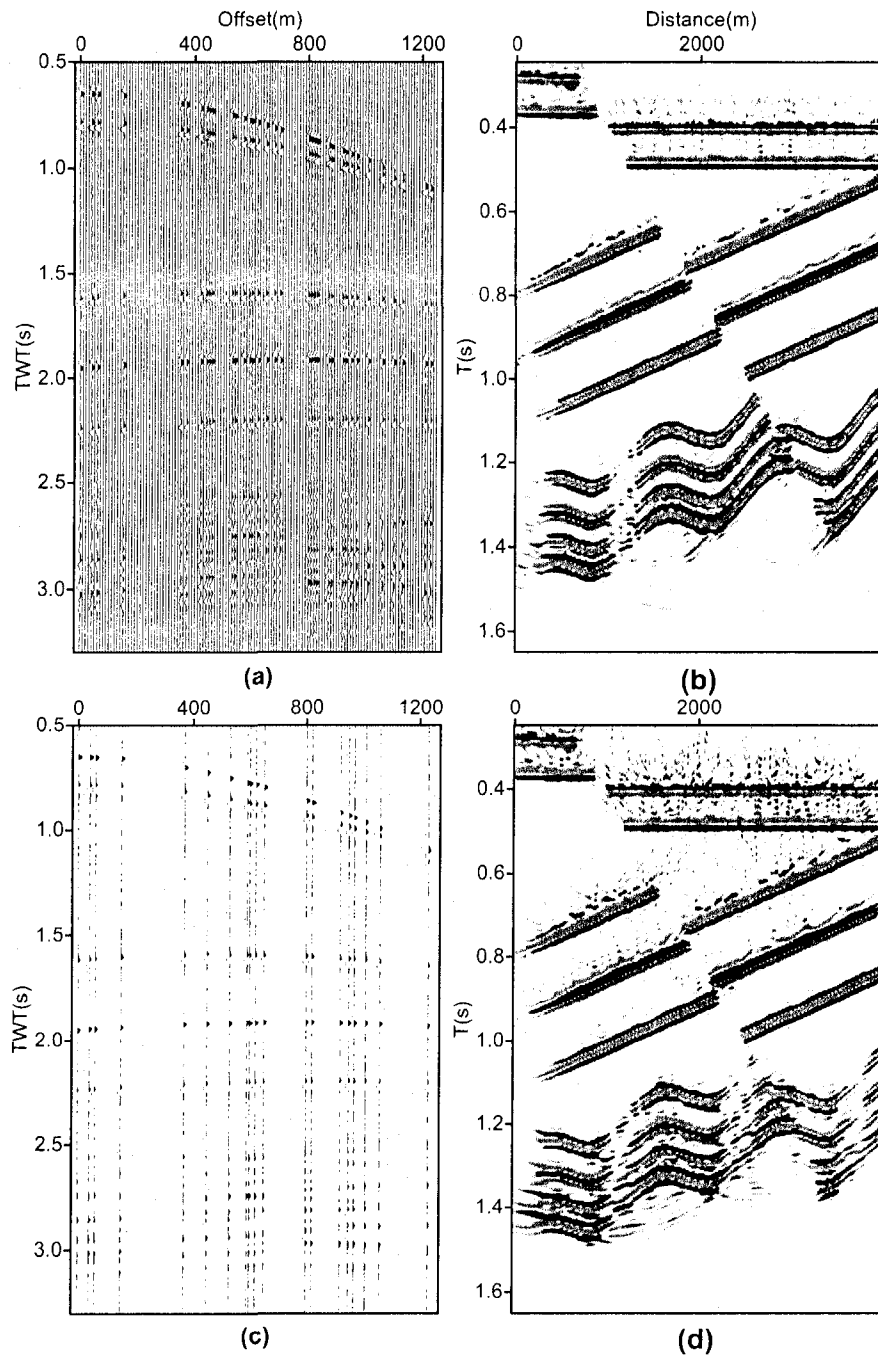


Figure 4.3: Migration with missing observations. a) and b) Decimated data with 75% of data removed and PSTM. c) and d) Decimated data with 90% of data removed and PSTM.

4.2 LS-PSTM of incomplete data

In equation (3.5) \hat{m} is a damped LS-PSTM image which is expected to be a de-blurred version of standard migration.

The LS-PSTM of the incomplete data is shown in Figure (4.4). The method of LS-PSTM increased the image resolution and the image is closer to the original model. The effect of wavelet has been removed as well as the source wavelet function was built in the forward operator. These images are the result of 30 iterations of the CG scheme. Figure (4.5) shows the convergence of CG method when 90% of data is removed. As it is expected, after 5 iterations the residual is decreased by 50%. There are two problems with LS-PSTM method in comparison to the conventional migration. First, the ability of LS-PSTM to increase resolution strongly depends on the accuracy of the velocity model. A wrong velocity model will prevent the method from convergence to a reasonable image. The second problem is the cost of the method. Each iteration in the CG is equal to two standard migrations, in addition both data and model are kept in memory as opposed to conventional migration where one trace at the time is placed in memory. The memory restriction is important and this is why this research required to use multi-processor systems with large memory.

4.2.1 Offset dependent regularized LS-PSTM of incomplete data

In the previous example I used damped least squares to produce LS-PSTM solutions. In this section, I introduce offset dependent regularization using regularization with the first order derivative operator. This is done by splitting the image in common image gathers and imposing offset dependent regularization. In other words, the unknown seismic image is now a function of migration time t_{mig} , lateral position x , and offset h . The model vector is now a function of 3 variables:

$$\mathbf{m} \rightarrow m(x, h, t_{mig}).$$

Common image gather (CIG) is a gather of NMO corrected traces from various offsets (or reflection angles) in time or depth. It is obtained by splitting the model vector $m(x, h, t_{mig})$ to $n \times x$ model with the dimension of $m(x = \text{constant}, h, t_{mig})$. In the other

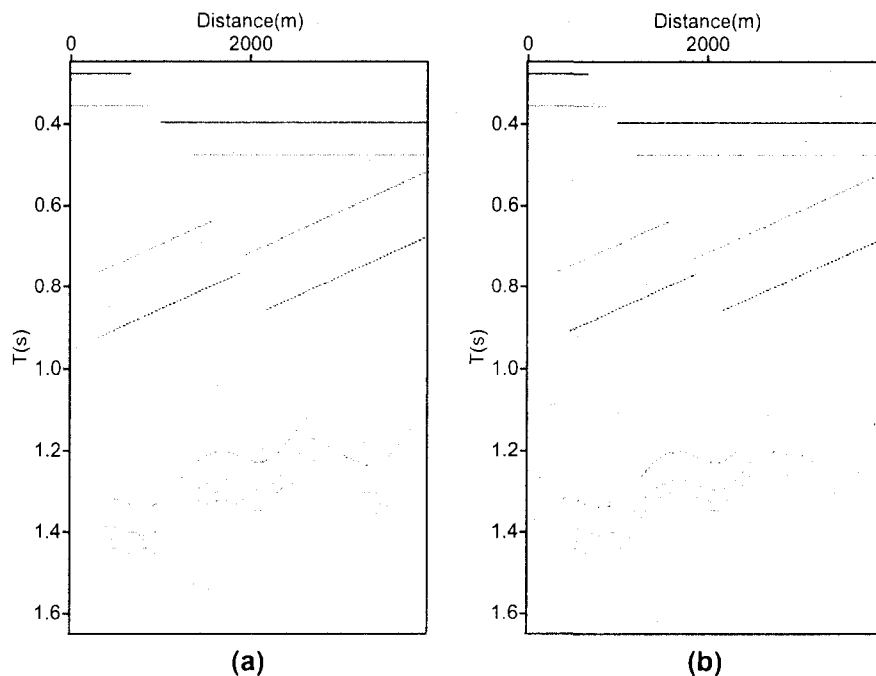


Figure 4.4: With incomplete data, resulted LS-PSTM has more resolution than standard migration and is comparable with the original model as in Figure (4.1). a) LS-PSTM when 50% of data is randomly removed. b) 90% of data is removed.

word all traces is a common image gather include information of the same subsurface position which may be offset-dependent.

If the velocities used for migration are correct, common image gathers should be composed of horizontal events. This is why we choose to use a regularization term that involves penalizing fast changes in the h axis for constant x . We will refer to this LS solution as the offset dependent regularized LS-PSTM solution. As always we use the available data to estimate a model of the subsurface by minimizing

$$\|d - \mathbf{Lm}\|^2 + \|D_{1/h_x} \mathbf{m}\|^2.$$

To investigate the effect of offset dependent regularization on the resolution enhancement of LSM, the LS-PSTM algorithm is applied on the aforementioned data set with 90% of data removed, and different amount of trade-off parameter.

Figure (4.7) shows the effect of using regularized LS-PSTM when applied to decimated data. Each gather includes 10 offset bins. Only two adjacent common offset gathers are shown. Figure (4.7)a shows the offset gathers without any regularization, and (4.7)b,c, and d show the cases with offset dependent regularization with trade-off parameters $\mu = 1, 10, \text{ and } 150$, respectively.

A large trade-off parameter causes more smoothness in the offset direction, and results in less artifacts in the migration image. Figure (4.6) shows the final image of the LS-PSTM without regularization and regularized LS-PSTM.

Figure (4.8) shows the effect of different values of the trade-off parameter on the convergence of LSCG algorithm. This figure shows that constraining the LS-PSTM (smoothing in the offset direction with a first derivative operator) changes the behavior of the LSCG convergence.

In Figure (4.8) we compare various inversion strategies. The case $\mu = 0$ represent no smoothing constraint. Decreasing μ from 50 to 10, 1, and .01, increases the speed of convergence. For $\mu = 0$, after 30 iterations, the residuals decrease about 20%, whereas for $\mu = 0.01$, the residuals decreases about 10%. Increasing the trade-off parameter does not improve the convergence, the quality of migrated section improves with smoothing but it becomes more difficult fitting the data.

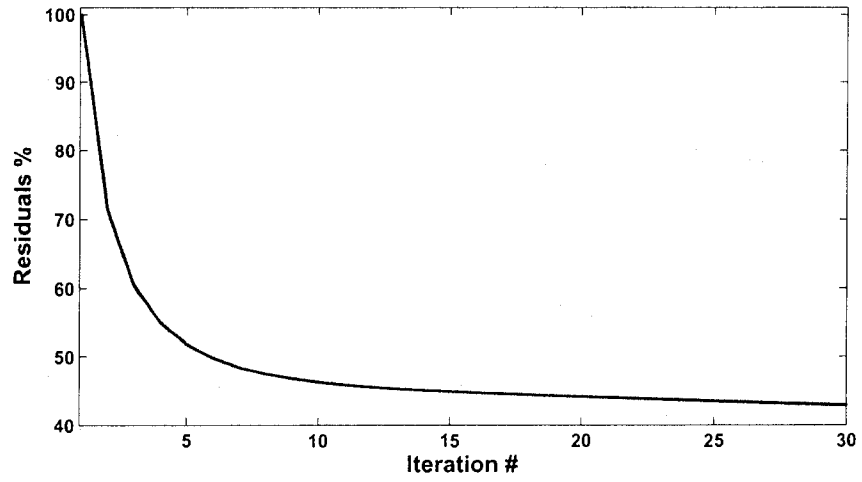


Figure 4.5: Convergence of LSCG method when only 10% of data is present.

4.2. LS-PSTM OF INCOMPLETE DATA

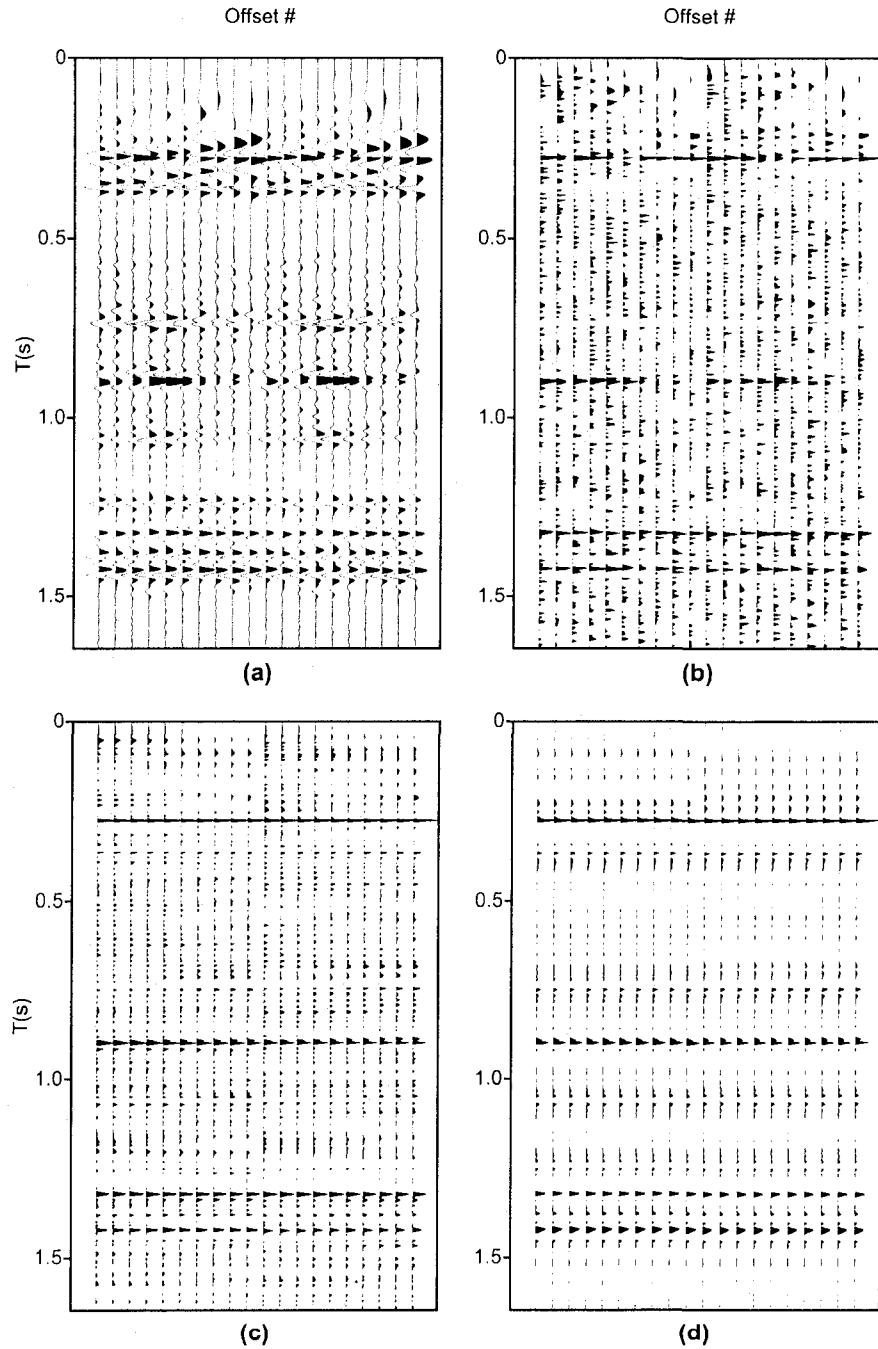


Figure 4.6: Effect of using regularized LS-PSTM on the estimation of common image gathers. Each gather corresponds to one midpoint position and 10 offset bins. a) CIG of PSTM. b) CIG of regularized LS-PSTM with $\mu = 1$, c) $\mu = 10$, and d) $\mu = 150$.

4.2. LS-PSTM OF INCOMPLETE DATA

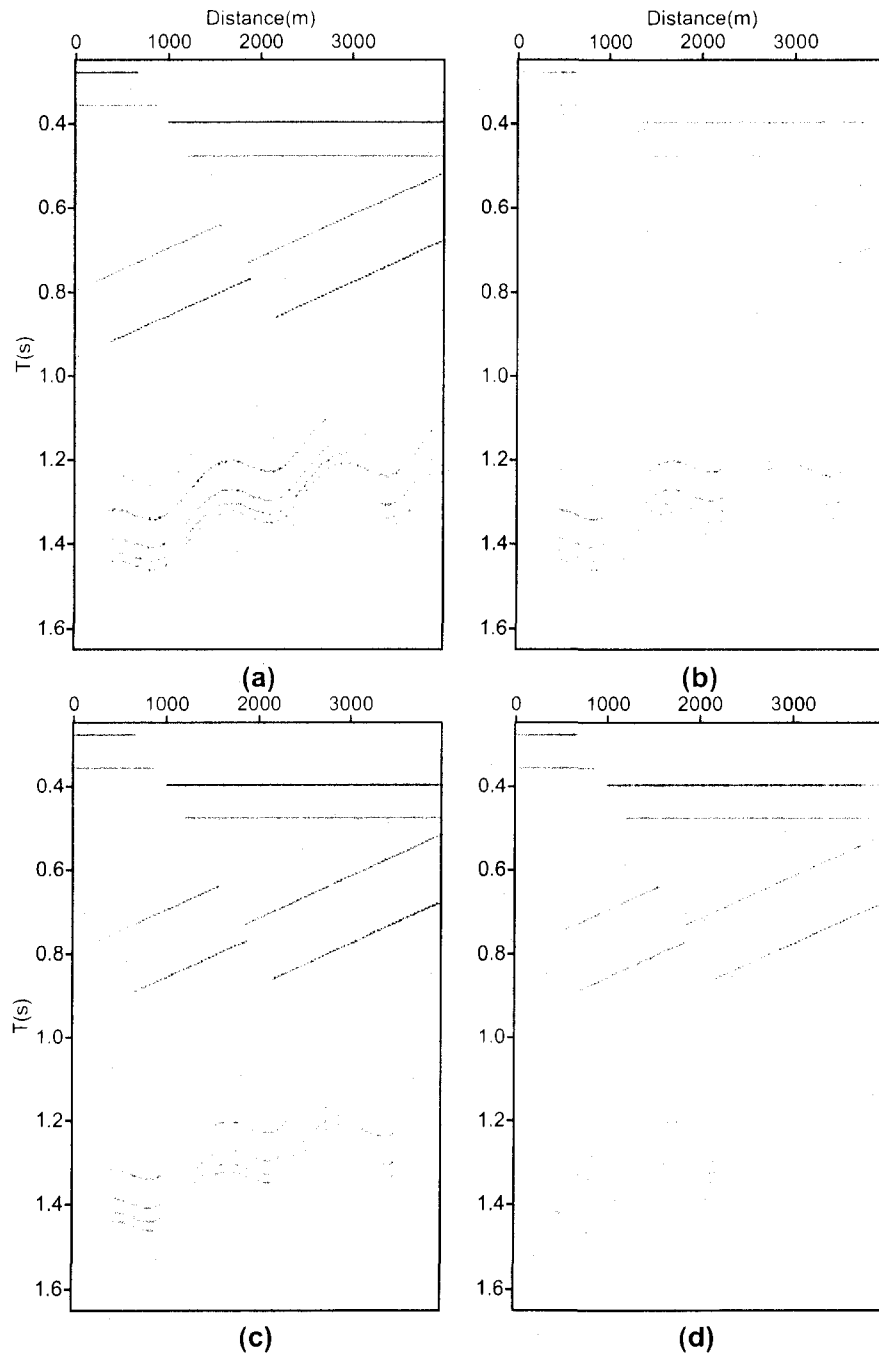


Figure 4.7: Effect of using offset dependent regularized LS-PSTM on the stack images. Each image is obtained by stacking common image gather along the offset dimension. a) Without regularization ($\mu = 0$), b) $\mu = 1$, c) $\mu = 10$, and d) $\mu = 150$.

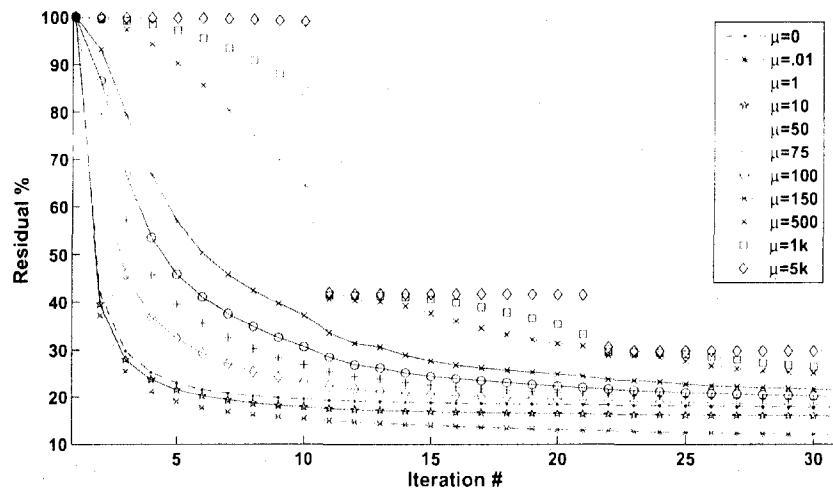


Figure 4.8: Convergence of offset dependent regularization LS-PSTM when 90% of the data are missing as a function of trade-off parameter μ .

4.3 Data reconstruction by LS-PSTM

Nearest neighborhood, linear and spline interpolation are the simplest seismic trace interpolation/extrapolation methods. Methods like Spitz (1991) and Porsani (1999) use properties of the Fourier transform for interpolation and are applied in the $F - X$ domain. Also Gulunay (2003)'s method is applied in the $F - K$ domain for spatial regularly sampled data.

Nemeth et al. (1999) proposed the LSM for reconstruction of missing data. This method is relatively expensive and the success of recovering data depends on operator and velocity precision.

The idea is that using a incomplete/irregular sampled data, it is possible to construct a reasonably high resolution LS-PSTM image as seen in the first parts of this chapter. If \mathbf{d}_I is considered as incomplete data and \mathbf{L}_I as the corresponding Kirchhoff forward modeling operator, then we have:

$$\mathbf{d}_I = \mathbf{L}_I \hat{\mathbf{m}}. \quad (4.1)$$

The regularized LSM with first derivative in the offset direction as a regularization, returns the de-blurred image, $\hat{\mathbf{m}}$, from this incomplete data:

$$\hat{\mathbf{m}} = (\mathbf{L}'_I \mathbf{L}_I + \mu^2 \mathbf{D}'_{1h_x} \mathbf{D}_{1h_x})^{-1} \mathbf{L}'_I \mathbf{d}_I. \quad (4.2)$$

The reconstructed data sets and the corresponding Kirchhoff forward modeling operator (\mathbf{d}_C and \mathbf{L}_C) can be are related via the following expression:

$$\mathbf{d}_C = \mathbf{L}_C \hat{\mathbf{m}}. \quad (4.3)$$

Replacing $\hat{\mathbf{m}}$ from equation (4.2) into equation (4.3) gives the formula for data reconstruction by regularized LS-PSTM:

$$\mathbf{d}_C = \mathbf{L}_C (\mathbf{L}'_I \mathbf{L}_I + \mu^2 \mathbf{D}'_{1h_x} \mathbf{D}_{1h_x})^{-1} \mathbf{L}'_I \mathbf{d}_I. \quad (4.4)$$

This method of data reconstruction is robust but it is relatively expensive. More missing data requires a large number of iterations for the same speed of convergence. On the

other hand more missing data makes the operator smaller and migration/de-migration faster. Strong dependency to the accurate velocity information is another disadvantage of the method.

4.3.1 Synthetics examples of data reconstruction via LS-PSTM

The aforementioned method of data reconstruction is used for reconstructing the 90% of removed traces from the synthetics data set showed in Figure (4.3 a). The offset dependent regularized LS-PSTM is used to estimate a de-blurred image of the earth reflectivity, the estimated image is used to reconstruct the data. Figure (4.9 a) shows a part of (125 traces) a shot gather from the data set including 80 shots, each has 140 receivers. Figure (4.9 b) shows the decimated data with 90% of the traces removed. Figure (4.9 c) shows the recovered data by the aforementioned method with $\mu = 150$. Panel (d) in Figure (4.9) is the difference between the true data and the reconstructed data. The difference between the original and reconstructed data mostly covered by random Gaussian noise added to the synthetic data. Most reflection events are modeled with the migration/de-migration operators and reconstructed data are almost free of random noise.

In order to measure of the difference between the reconstructed data using method of regularized LS-PSTM, and the observations (true data), the root-mean-square (RMS) errors is calculated for different trade-off parameters. Figure (4.10) shows the result. The minimum RMS error corresponds to $\mu = 150$. Increasing μ gives a smoother image of LS-PSTM, however, it does not improve the data reconstruction. The reconstructed data are shown in Figure (4.9).

4.3. DATA RECONSTRUCTION BY LS-PSTM

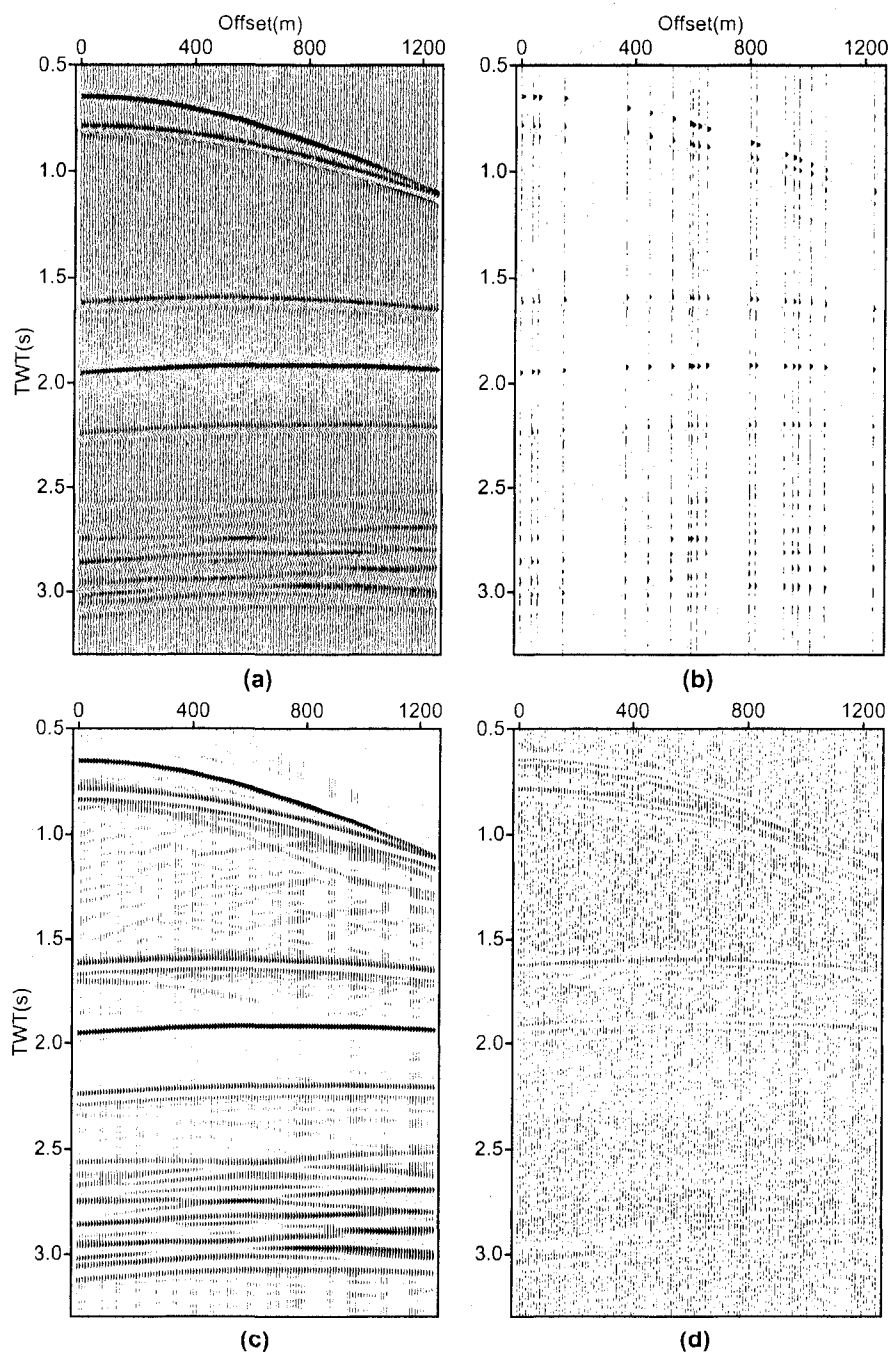


Figure 4.9: Data reconstruction by offset dependent regularized LS-PSTM for the synthetic model of Figure (4.1). a) Original data. b) Decimated data with 90% of the data removed. c) The reconstructed data. d) Error panel or difference between original and reconstructed data.

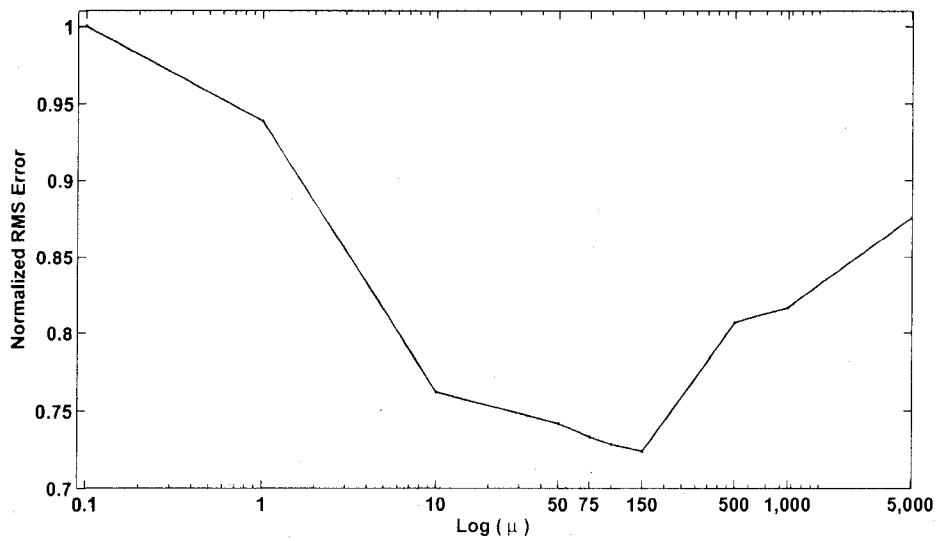


Figure 4.10: RMS error for data reconstruction by offset dependent regularized LS-PSTM for the synthetic model of Figure (4.1) versus trade-off parameter, μ . The best data reconstruction is obtained when $\mu = 150$. The reconstructed data are shown in Figure (4.9).

4.4 LS-PSTM and data reconstruction of the Marmousi data set

The Marmousi data set is an example of a complex 2D synthetic model. This data set was created by Institut Francais Petrole (IFP) and presented in the 52nd meeting of the European Association of Geoscientists and Engineers (EAGE) as a benchmark for a workshop on practical aspects of seismic inversion (Versteeg, 1993).

The Marmousi model was inspired by the complex geology of the Cuanza basin in North Quenguela, Angola. A streamer data acquisition was simulated via a 2D acoustic finite difference modeling program (Versteeg, 1993). The Cuanza basin has strong horizontal and vertical velocity variation, with velocities ranging from $1500m/s$ to $5000m/s$.

The Marmousi Data set includes 240 shots and 96 receivers per shot. This amounts to a total of 23040 seismograms or traces. The receiver spacing is $25m$ and the simulated recorded time is $2.9sec$ with a $4ms$ sampling interval (725 samples per trace) that corresponds to a Nyquist frequency of 125 Hz. This model is shown in Figure (4.11)(a).

Both the structural complexity and the strong velocity variation make the Marmousi model a challenging benchmark to test migration and inversion methods. It is important to stress that raytracing and Prestack Depth Migration are necessary tools to give a reasonably true image of subsurface earth reflectivity for this data set. In this thesis, I have tested the ability of LS-PSTM for data reconstruction. It is clear that the algorithm I have constructed (time migration algorithm) is not optimal for this type of data sets. It is important to stress, however, that prestack migration implemented via LS-PSTM is less expensive than a depth domain implementation and also it is less sensitive to the velocity model than depth imaging. If one is interested in obtaining an accurate image of the subsurface then a depth imaging code is in order for this particular data set. However, if one relaxes the need of high accuracy imaging, and is concerned with data reconstruction, LS-PSTM seems to be a good compromise between accuracy in the reconstruction and computational cost.

The original velocity model is given by a grid of $4m \times 4m$. In order to have a smoother model with grid size, the velocity field was convolved with five point smoothing operator (0.25, 0.5, 0.75, 0.5, 0.25) in both the vertical and horizontal directions.

In order to show the ability of method to reconstruct data from complex models, I

4.4. LS-PSTM AND DATA RECONSTRUCTION OF THE MARMOUSI DATA SET

removed half of data by removing one trace and leaving the next one. Figure (4.11) (b,c) shows the PSTM and LS-PSTM image solutions. Comparing images it is clear that the image obtained via LS-PSTM has higher resolution than the image obtained via classical migration. In addition, the LS-PSTM image is less contaminated by sampling artifacts.

Figures (4.12) show the data reconstruction of the Marmousi data set. Figures (4.12) (a), (b), (c), and (d) are the complete data (for shot record 230), incomplete data, reconstructed data, and difference between true and reconstructed data, respectively.

The method is able to reconstruct the most energetic seismic events. However, because we have chosen a time-migration implementation, our algorithm can only recognize hyperbolic events, and therefore, not all the reflections were properly modeled.

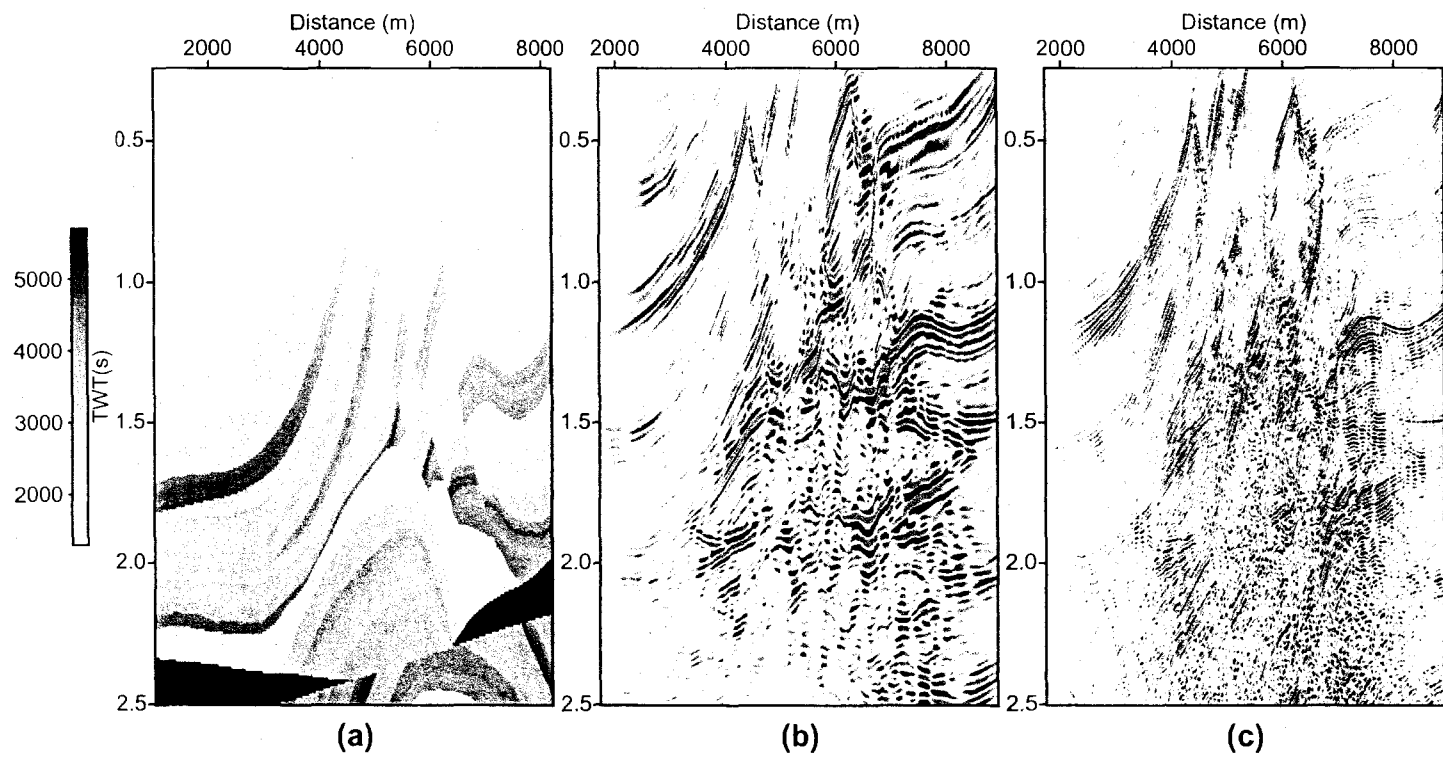


Figure 4.11: The Marmousi synthetic model. a) Velocity model. b) Image obtained by migrating the decimated data with PSTM. c) Image obtained by migrating the decimated data with LS-PSTM.

4.4. LS-PSTM AND DATA RECONSTRUCTION OF THE MARMOUSI DATA SET

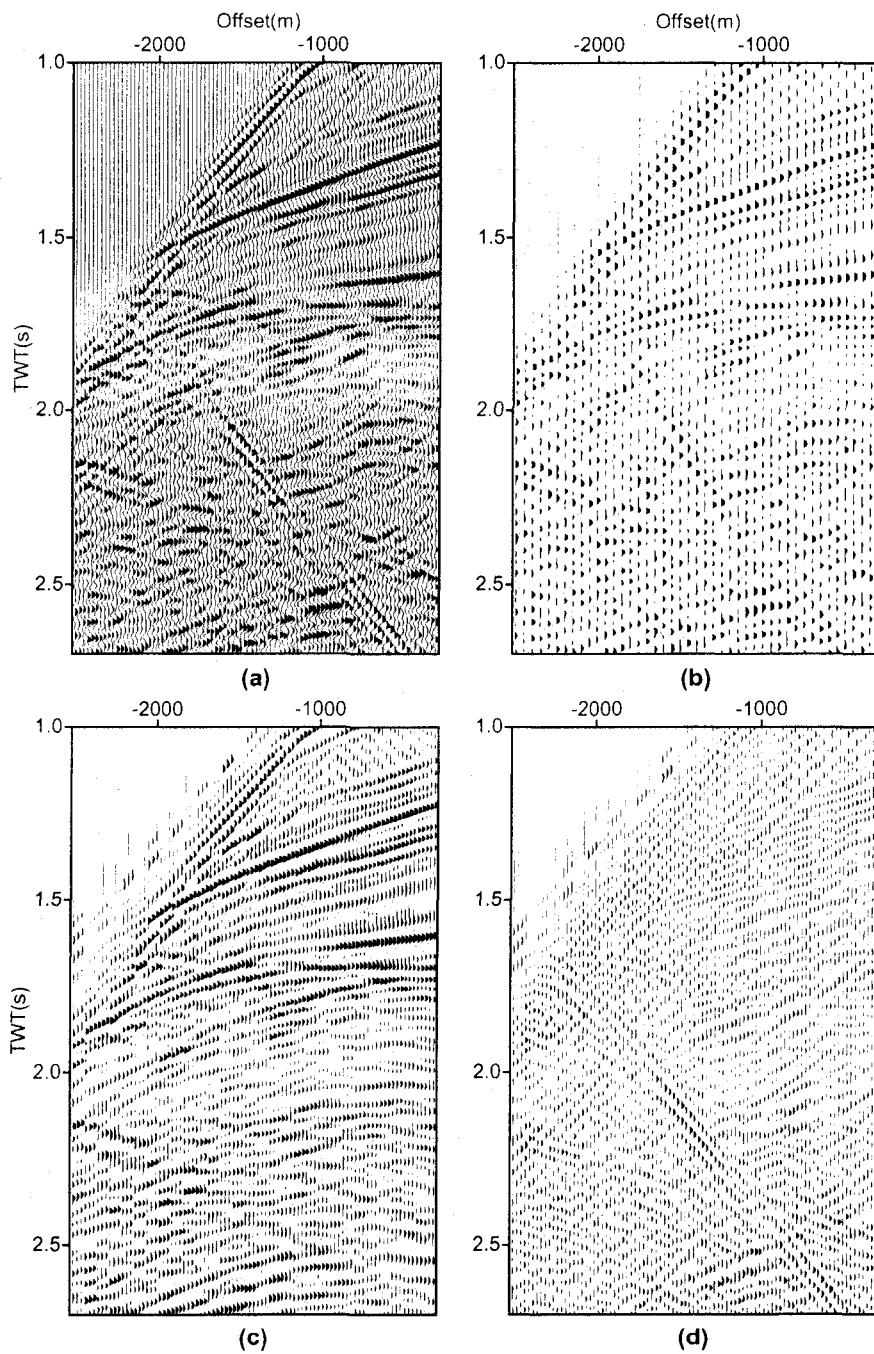


Figure 4.12: Data reconstruction for Marmousi data set. a) Original data, in this case field record 230. b) Decimated data with 50% of traces removed. c) Reconstructed data. d) Error panel or difference between original data and reconstructed data.

4.5 Dependency of LS-PSTM data reconstruction on velocity information

In Kirchhoff time migration (and also in the other migration methods), velocity is an inseparable part of migration equations. Prestack Kirchhoff time migration practically uses equation (2.22). In equation (2.22), V is the velocity of the medium, which can be replaced by RMS velocities, V_{RMS} .

To show the effect of small inaccuracy in velocity information on migration, the data set portrayed in Figure (4.2 a) was migrated with velocities that were perturbed $\pm 10\%$ with respect to the true velocity model. The results of standard migration are shown in Figure (4.13). Comparing the results of migration with the true velocity model in Figure (4.2 b) and with $\pm 10\%$ error in Figures (4.13 a,b), one can appreciate the importance of having an accurate velocity model for migration.

The LS-PSTM reconstruction algorithm was tested with the perturbed velocity model as well. We examine the case where 90% of the data were removed (Figure (4.14)). The reconstruction algorithm uses offset dependent regularized LS-PSTM with the number of iterations equal to 30. Figures (4.14 a and b) show the reconstructed data and (4.14 c and d) show the difference between original and reconstructed data. Comparing these figures with Figures (4.9 c and d) shows that the problem with data reconstruction is that reconstructed events are not in the right position. This is a consequence of using the wrong velocity model. It is clear that seismic data reconstruction using LS-PSTM requires accurate velocity models. This is not unexpected; the velocity information is an integral part of the operator that models the data.

4.6 Summary

Irregular or incomplete data introduces artifacts in Kirchhoff PSTM. The LS-PSTM algorithm can be used to minimize sampling artifact in migrated images.

High resolution images computed via LS-PSTM can be used for data reconstruction. In this chapter, I showed the effect of using LS-PSTM and regularization on the resolution enhancement of migrated image. Two synthetic examples were used to test the feasibility of the method for velocity dependent seismic data reconstruction.

4.6. SUMMARY

The reconstruction of the Marmousi data shows that time-domain algorithms are not sufficient for data arising from complex velocity models. A least-squares prestack depth migration (LS-PSDM) is required in situations of high structural complexity.

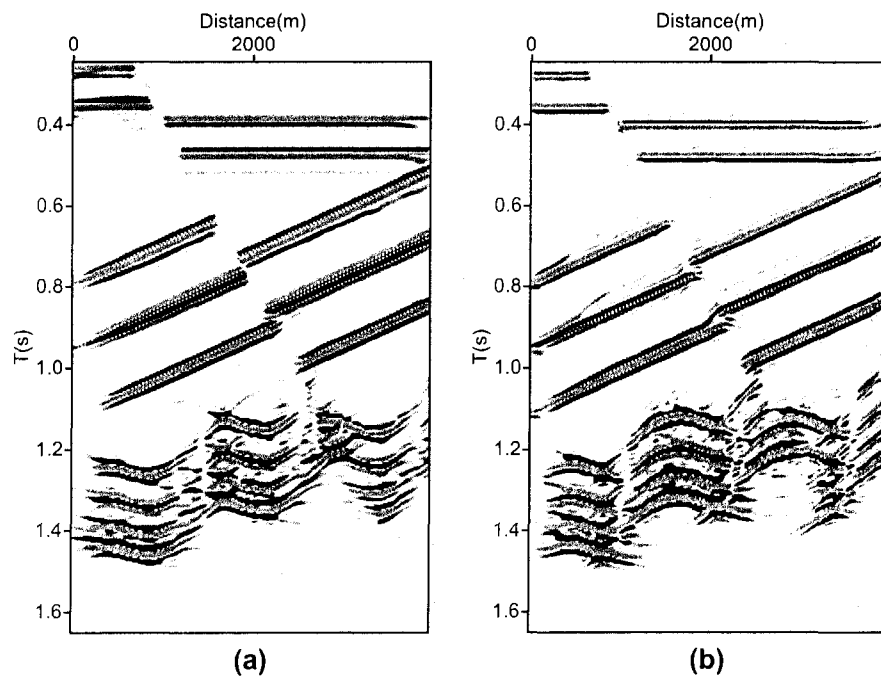


Figure 4.13: Effect of inexact velocity information on Kirchhoff PSTM. a) 10% velocity error. b) -10% velocity error. The image obtained with the correct velocity model is displayed in Figure (4.2 b)

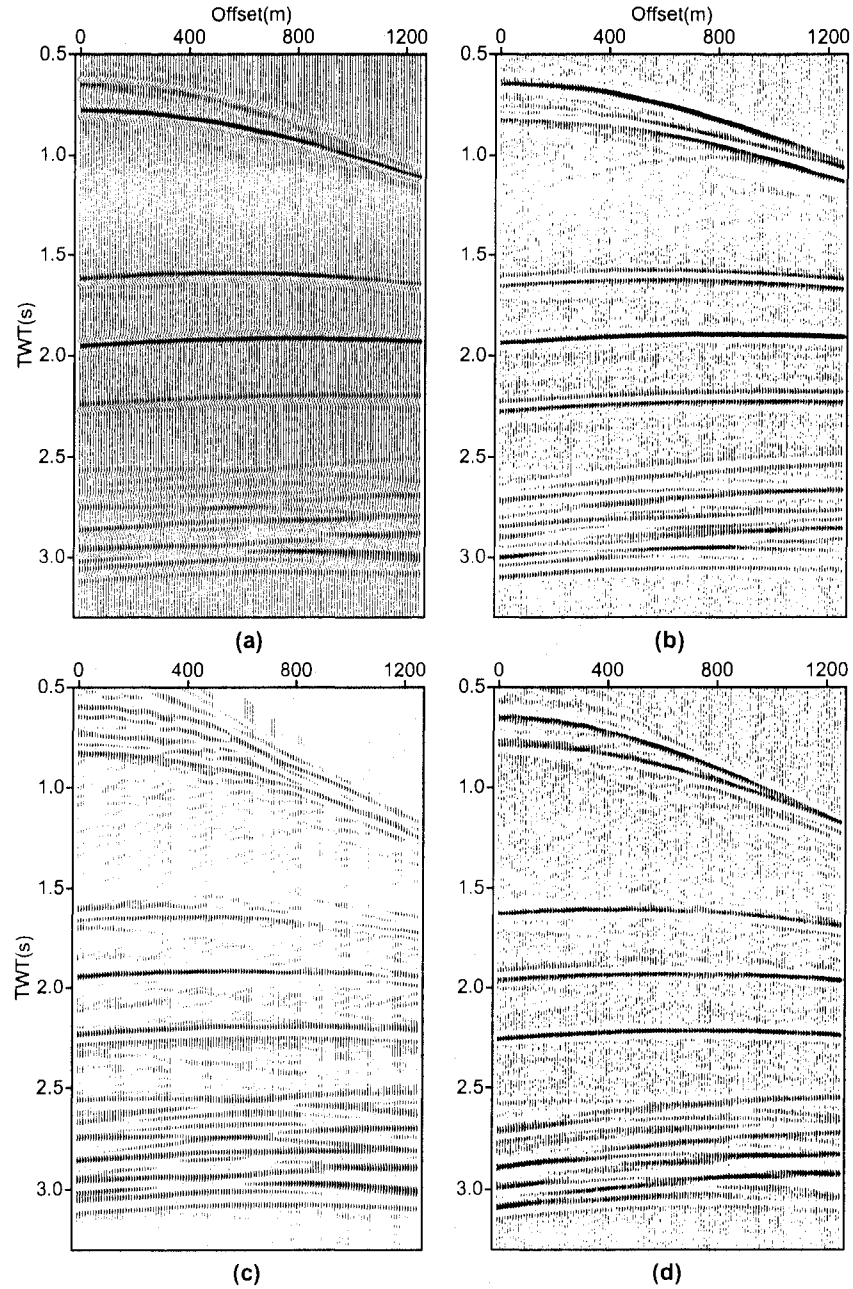


Figure 4.14: Effect of inexact velocity information on data reconstruction. a) Reconstructed data with 10% velocity error. b) Reconstructed data with -10% velocity error. Error panels for a) and b) are shown in panels c) and d), respectively.

Chapter 5

PSTM, Regularized LS-PSTM and Data Reconstruction of Real Data

5.1 Gulf of Mexico data set

The Gulf of Mexico data set is a long 2D seismic line acquired over a shallow salt pillow in deep water (1500m). The Gulf of Mexico data set with its strong multiples is a typical marine data set. This data set was distributed at the workshop on Comparison of Seismic Multiple Attenuation Techniques held at the SEG's annual meeting in 1997 (Vreschuur and Prein, 1999).

In the Gulf of Mexico data set, multiples are generated by both, the hard deep sea floor, and the tabular salt body. Variable strength of multiples and weak primaries cause multiple removal and consequently, imaging of subsalt layers a problem. Figure (5.1) shows the stacked section of this data set after a processing flow that does not include multiple attenuation.

Strong first order multiples are seen at 3.2, 3.7, 4.4, and 5sec in the middle and right-hand side of the image. After 6sec a series of second order multiples are visible (Vreschuur and Prein, 1999). Also, diffraction hyperbolas with apex at 2.3sec are detectable. Strong multiples make the identification of primaries a difficult task. This is particularly true under the salt pillow (2.3sec to 2.8sec in the middle and right-hand side of the image.)

The available data set donated to the Signal Analysis and Imaging Group (SAIG) consists of 810 marine (end-off) shot-records. Each shot-record has 183 receivers, leading to

5.1. GULF OF MEXICO DATA SET

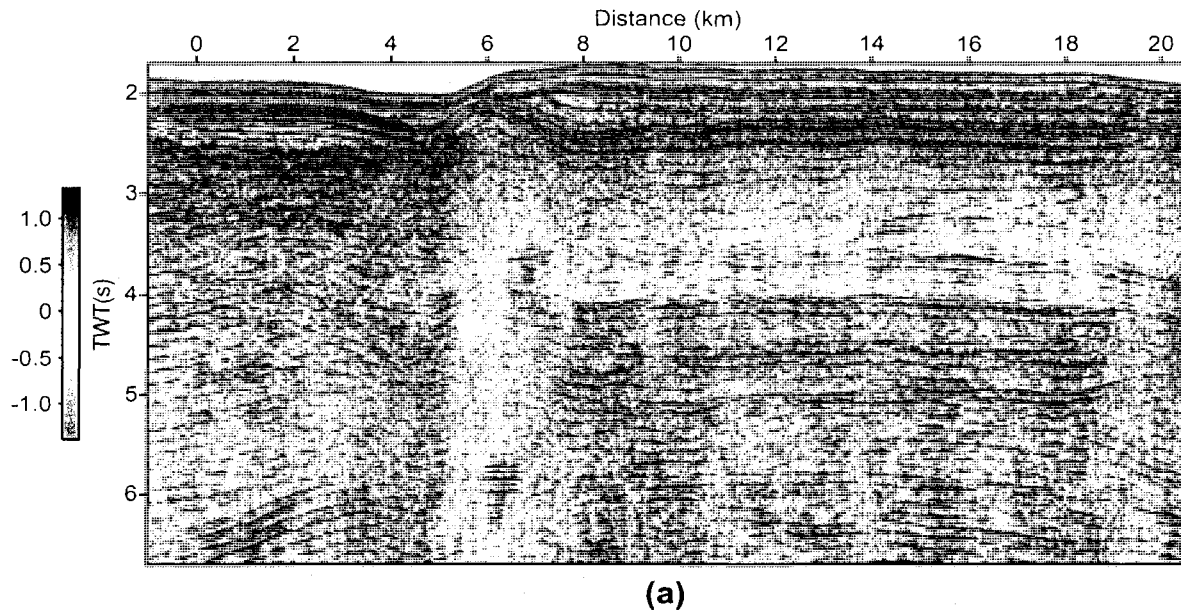


Figure 5.1: Stacked section of the Gulf of Mexico data set. Processed with the Seismic Unix software prior to multiple attenuation. Strong first order multiples are visible at 3.2, 3.7, 4.4, and 5 sec in the middle and right-hand side of image. After 6 sec another series of multiples are visible.

148220 traces in 1800 CDP (Common Depth Point) gathers. The first CDP is numbered as 818, and the first shot-record numbered, is the shot-record 45. CDPs started at the position of $-2437m$ and ended at the position of $24003m$, with $13.335m$ interval in between. Recording time is $7sec$ with $4ms$ time sampling interval and 1751 samples per trace.

In this chapter we demonstrate the use of PSTM and LS-PSTM to produce an image of the subsurface for this data set. In addition, we discuss the data reconstruction problem with the addition of one complication: the data is severely contaminated by multiple reflections which are not modeled by the de-migration and migration operator. We also investigate PSTM and LS-PSTM after and before multiple attenuation via the parabolic Radon transform.

5.2 Velocity analysis and multiple attenuation

In seismic imaging, one basic assumption is that multiple reflections have been removed (or at least attenuated) from the recorded data. There exists many methods to attenuate multiples. Each of these methods is restricted to its assumptions or prerequisites. A classification of multiple removal methods is provided by Weglein (1999) who divides them in two main categories:

1. Filtering methods which seek for some features or properties in the data that are different in multiples and primaries. Predictive deconvolution is an example of a filtering method. Radon transforms, stacking, eigenimages and Fourier transform which all are based on separability of multiples from primaries in a surrogate domain are another examples of filtering methods (Weglein, 1999).
2. Prediction methods that try to predict and then subtract multiples from data. These methods predict multiples using modeling or inversion of seismic wavefields. Wavefiled extrapolation, feedback loops, and inverse scattering series are examples of prediction methods (Weglein, 1999).

The multiple removal method proposed by Liu (1996) and Nemeth et al. (2000) (LSM multiple attenuation) can be placed in the first category. They modeled both primaries, as well as multiples, and then subtract the multiples from the data.

As it was mentioned in Chapter 2, Kirchhoff migration and modeling do not account for multiples. However, multiples will remain in the migrated image when their Move-Out is close to the primaries' MoveOut or they are strong enough to mask primaries.

Subsequently, when strong multiples are present in the data, Kirchhoff LS-PSTM is not able to improve the quality of the subsurface image. In this chapter, PSTM and LS-PSTM of data before and after multiple attenuation are studied. We will clearly show the importance of de-multiple prior to imaging.

5.2.1 Parabolic Radon Transform

The parabolic Radon transform is used to remove multiple reflections. The parabolic Radon transform was introduced for multiple attenuation by Hampson (1986). After

5.2. VELOCITY ANALYSIS AND MULTIPLE ATTENUATION

NMO correction, the residual move out of the seismic reflection events can be approximated by parabolas. In a CDP gather, the traveltime t for an event at offset h , with the velocity V , and zero-offset traveltime τ , is calculated via the following expression

$$t = \sqrt{\tau^2 + \frac{h^2}{V^2}}. \quad (5.1)$$

After NMO correction, using velocity V_{NMO} , the events shift up by the amount of Δt :

$$\Delta t = \sqrt{\tau^2 + \frac{h^2}{V_{NMO}^2}} - \tau. \quad (5.2)$$

Therefore, the travel time of the NMO corrected data will be given by the following expression (Moldoveanu, 2006)

$$t = \sqrt{\tau^2 + \frac{h^2}{V^2}} - \left(\sqrt{\tau^2 + \frac{h^2}{V_{NMO}^2}} - \tau \right), \quad (5.3)$$

which, after expanding the last expression via a Taylor series, one arrives to the parabolic travel-time equation

$$t = \tau + ph^2. \quad (5.4)$$

where

$$p = \frac{1}{2\tau} \left(\frac{1}{V^2} - \frac{1}{V_{NMO}^2} \right). \quad (5.5)$$

is the curvature of the reflection after NMO correction (Moldoveanu, 2006). Summation of all amplitudes along the parabolic trajectories transforms the data into the parabolic (τ, p) domain. In this new domain the primaries are separable from the multiples.

For multiple attenuation, the NMO correction is applied to CMP gathers, and then the Radon transform is used to map the data to the (τ, p) space. In the (τ, p) domain,

5.3. PSTM AND LS-PSTM AND RECONSTRUCTION PRIOR TO MULTIPLE ATTENUATION

primaries are muted, and then by transforming back to the original domain, one obtains an estimate of the multiples. The modeled multiples are finally subtracted from the data.

Low ratio of primaries to multiples in the Gulf of Mexico data set cause velocity analysis to be problematic. Figure (5.2 a) shows the velocity semblance for CDP gather 2100. High amplitude events with velocity less than $1500m/sec$ are produced by multiples.

Figure (5.2 b), on the other hand, shows the stacking velocity semblance for the same CDP gather after multiple attenuation.

Using the Seismic Unix software (CWP, 1984), velocity analysis is performed on a selected CDP gathers and the results were extrapolated to all the area. Then the parabolic Radon transform is used for multiple attenuation of NMO corrected data. After that, the data underwent an inverse NMO. Figure (5.3) shows the result of this procedure in the field record 647. Figure (5.3) (a), (b), (c), and (d) show this shotgather before NMO correction, after NMO correction, after multiple attenuation, and after applying inverse NMO, respectively.

In the resulted shotgather, (Figure 5.3 d), strong multiples are attenuated especially in the depths below $3.5sec$. Stacking velocity semblance of this shotgather, (Figure 5.2, b), shows that there is not any strong event in the depths more than $3sec$ with the semblance velocity less than $1500m/sec$, which is a little more than the speed of sound in water.

5.3 PSTM and LS-PSTM and reconstruction prior to multiple attenuation

I performed PSTM and LS-PSTM with the velocity information acquired by the analysis of stacking velocities. PSTM is performed on the raw data with 50% of the shot records removed. Figures (5.4) (a) and (b) show the images obtained via PSTM and LS-PSTM with 20 conjugate gradients iterations, respectively. A comparison of Figures (5.4) and (5.1) shows that LS-PSTM has produced an image with higher temporal resolution. This is due to the fact that source wavelet removal is incorporated into the inversion process. One problem with these images is that the multiples, not modeled by the de-migration and the migration operators, are leaking into the final images. In other words, the images are corrupted by events that were not considered in the formulation of the imaging

5.3. PSTM AND LS-PSTM AND RECONSTRUCTION PRIOR TO MULTIPLE ATTENUATION

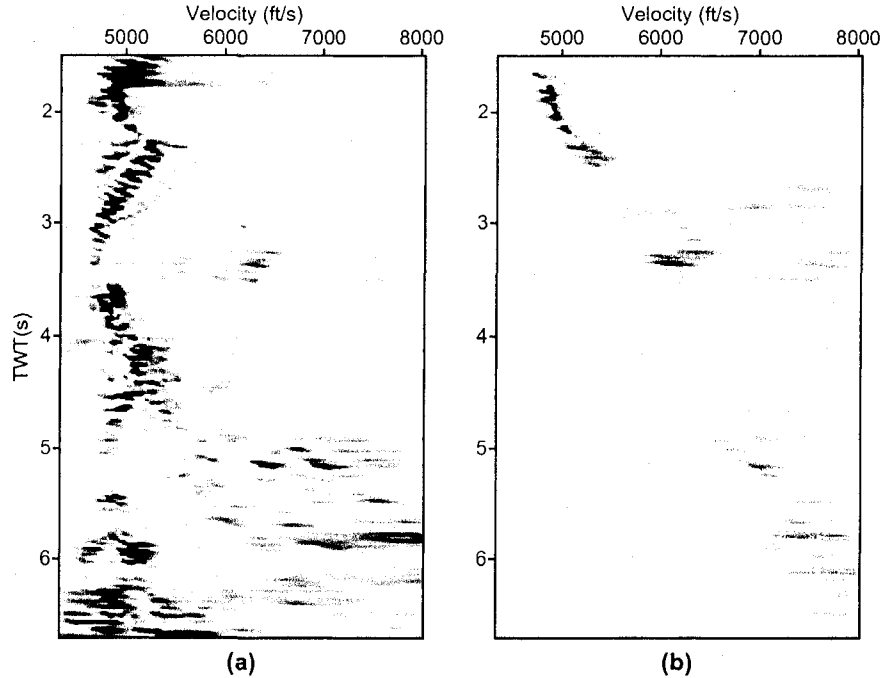


Figure 5.2: Velocity analysis using semblance analysis for the CDP 2100 from the Gulf of Mexico data set. a) Velocity analysis of the original data. b) Velocity analysis of the data after removing multiples using the Radon transform.

operator.

Figure (5.5) shows data reconstruction of shotgather 647. Half of the original data (shotgathers with odd numbers) have been removed. Figures (5.5) (a), (b), (c), and (d) show the original shot gather 647, the decimated gather, the reconstructed shot gather, and the difference between original and reconstructed data, respectively. The difference in Figure (5.5)(d) shows that many events were not modeled. These events may be multiples in the original data plus coherent signals arising from improper modeling of primary signals.

In order to see if the events which are not modeled during data reconstruction correspond to the multiples or not, Figure (5.6) compares the extracted multiples by the Radon transform, (Figure 5.6 a), and the differences between the original data and the reconstructed data using LS-PSTM, (Figure 5.6 b). Figure (5.6 c) shows that the residual

5.3. PSTM AND LS-PSTM AND RECONSTRUCTION PRIOR TO MULTIPLE ATTENUATION

events in the difference are not necessarily multiples. However, the failure of data reconstruction is due to the presence of multiples. As we will show in the next section, after multiple attenuation, data reconstruction of is more successful.

5.3. PSTM AND LS-PSTM AND RECONSTRUCTION PRIOR TO MULTIPLE ATTENUATION

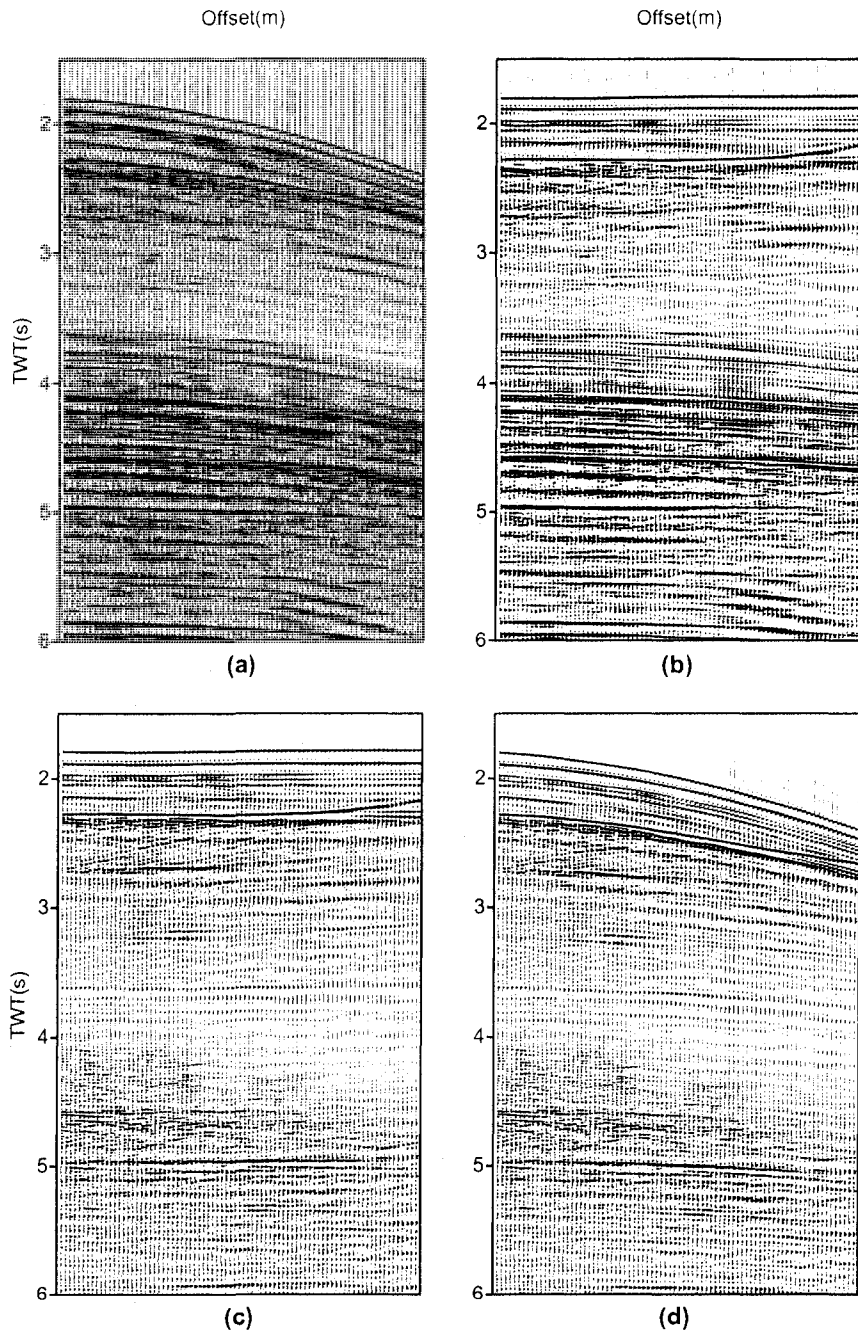


Figure 5.3: Multiple removal from the Gulf of Mexico data set, field record 647. a) Original data with strong multiples. b) NMO corrected data. c) Data after multiple attenuation. d) Data after inverse NMO correction.

5.3. PSTM AND LS-PSTM AND RECONSTRUCTION PRIOR TO MULTIPLE ATTENUATION

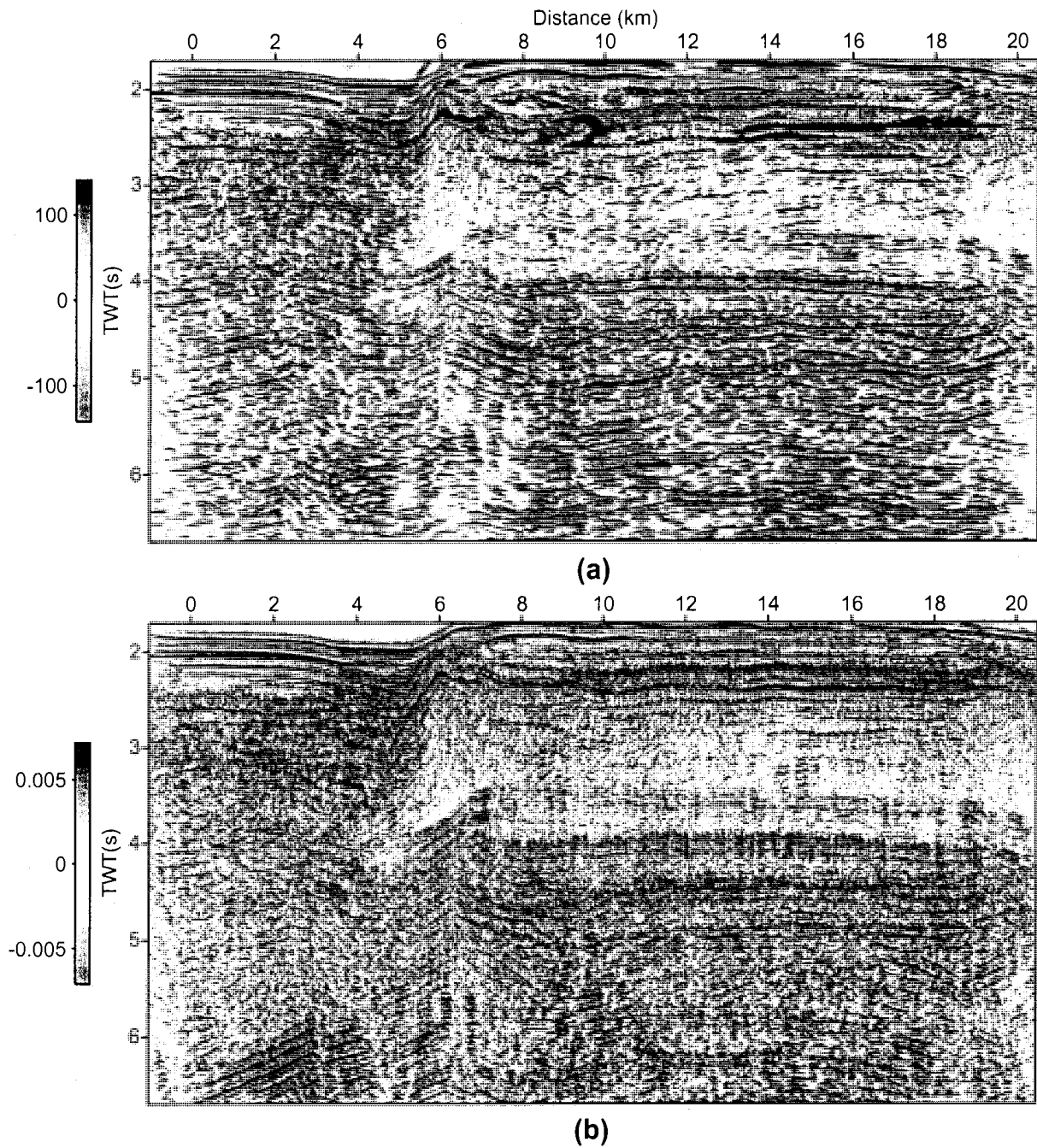


Figure 5.4: Migration images of the Gulf of Mexico data set with 50% of shot records removed. a) PSTM subsurface image. b) LS-PSTM image.

5.3. PSTM AND LS-PSTM AND RECONSTRUCTION PRIOR TO MULTIPLE ATTENUATION

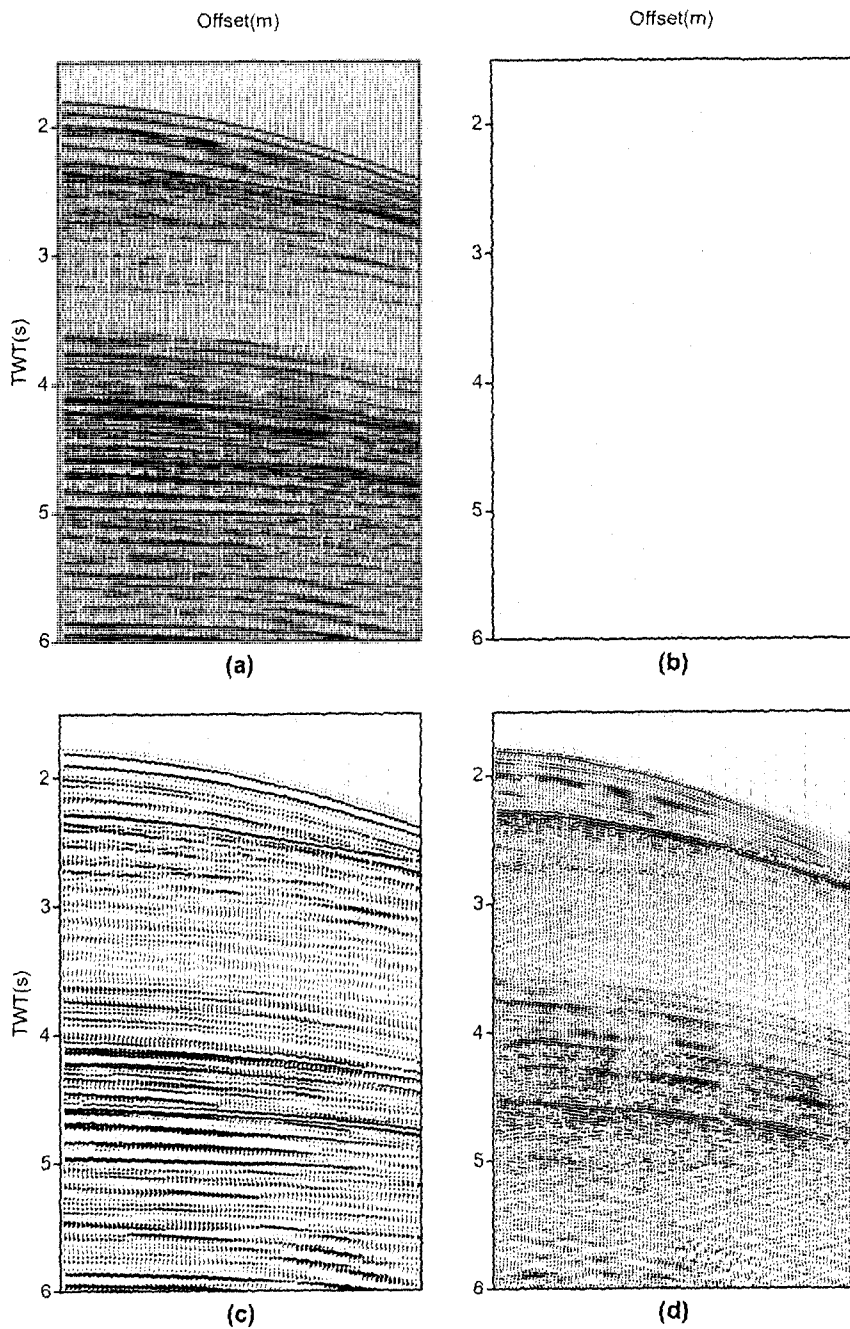


Figure 5.5: Data reconstruction of Gulf of Mexico data set. Multiples are present in the original data. a) The original data displaying shotgather 647. b) Decimated data. c) Reconstructed shotgather. d) Difference between original and reconstructed data.

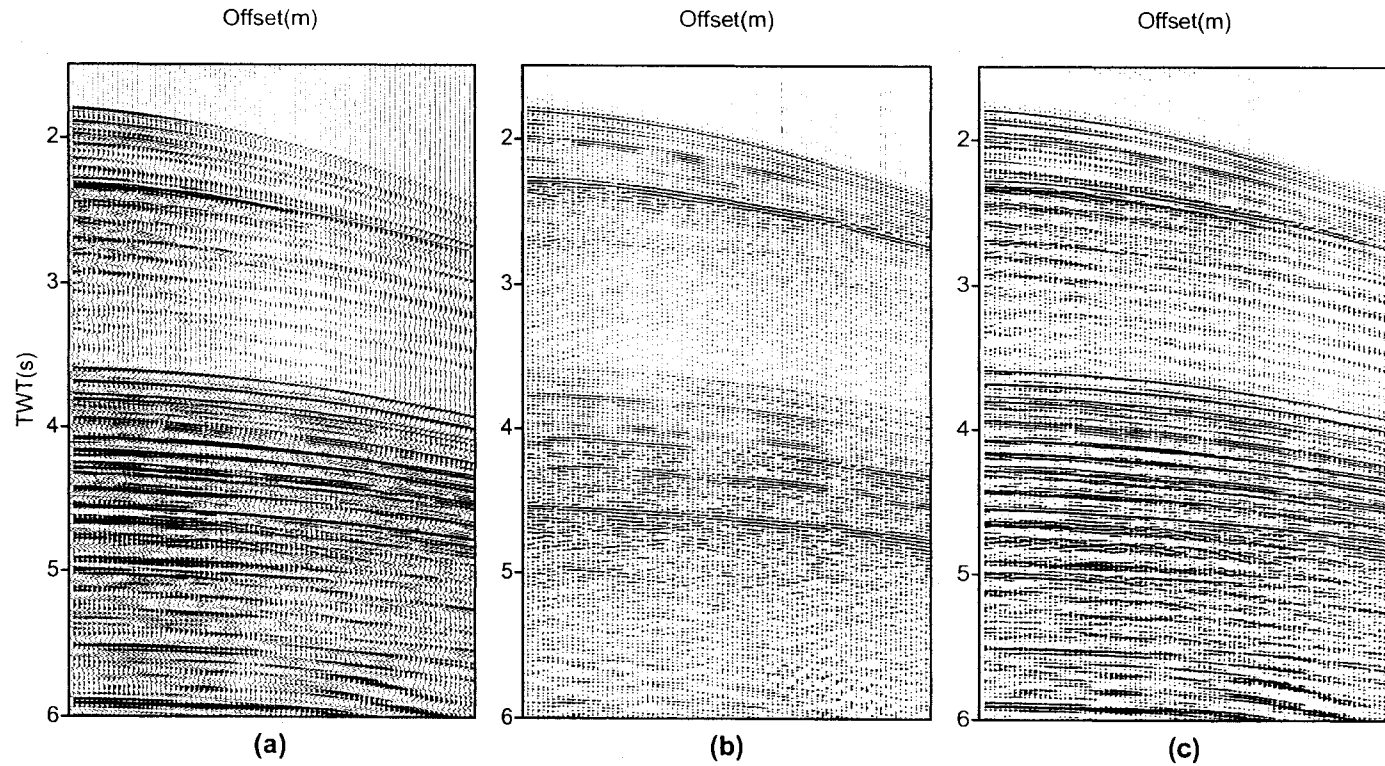


Figure 5.6: Comparison between multiples and un-constructed events in the process of data reconstruction of the row data. Field record 647, a) Estimated multiples using RT (the differences between original data (Figure 5.3 a) and demultiplied data by RT (Figure 5.3 d)). b) Un-constructed events in the data reconstruction (Figure 5.5 d). c) Difference between a) and b).

5.3. PSTM AND LS-PSTM AND RECONSTRUCTION PRIOR TO MULTIPLE ATTENUATION

The CIG associated to CDP 2100, are portrayed in Figures (5.7)(a) and (b) for PSTM and LS-PSTM, respectively. Multiples present in the data show themselves in the common image gathers as parabolic events. These strong non-horizontal events prevent the effect of smoothing in the offset direction to be effective in the improvement of subsurface image. In other words, as we have already mentioned, the multiples were not include in the operator (L) and therefore, they will corrupt the image estimated via LS-PSTM.

5.3. PSTM AND LS-PSTM AND RECONSTRUCTION PRIOR TO MULTIPLE ATTENUATION

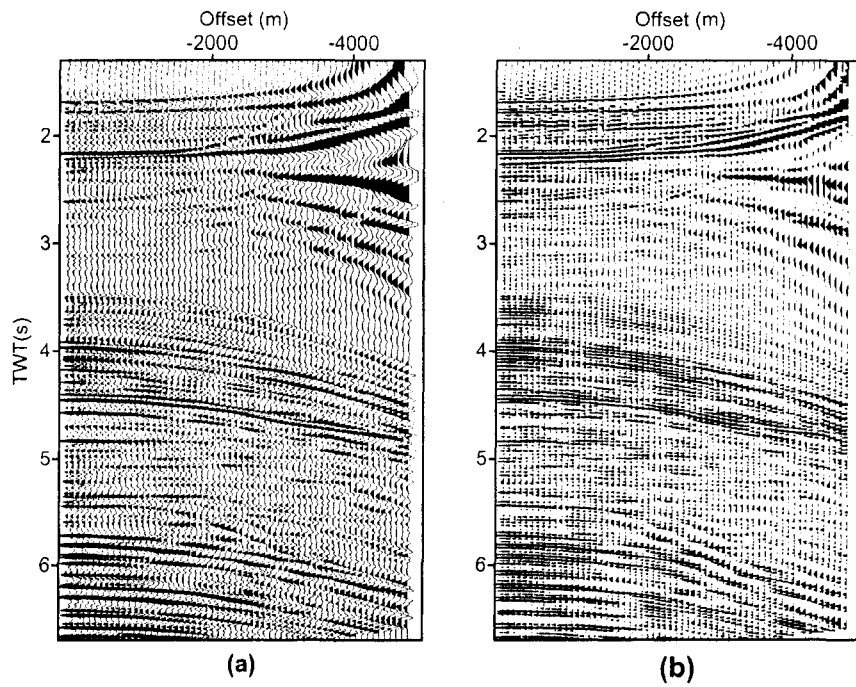


Figure 5.7: CIG of CDP 2100 of the Gulf of Mexico data set. The multiples show themselves as parabolic events, therefore performing smoothness in the offset direction is not effective. a) PSTM. b) LS-PSTM.

5.4 Regularized LS-PSTM and data reconstruction after multiple attenuation

With the same velocity information as in the previous section, PSTM and LS-PSTM are performed on multiple attenuated data. In both cases 50% of the shot records were removed to simulate a sub-optimal acquisition. Figures (5.8) (a) and (b) show the images obtained via PSTM and LS-PSTM (20 iterations).

Comparing the results of PSTM when multiples are attenuated (Figure 5.8 a) with PSTM prior to multiple attenuation (Figure 5.4 a) shows an important improvement in image quality.

The image obtained via LS-PSTM is used for data reconstruction. Figure (5.9) shows data reconstruction of shotgather 647 when half of original data (shotgathers with odd numbers) were removed. Figures (5.9) (a), (b), (c), and (d) show the original shot gather, the decimated gather, the reconstruction, and the error panel, respectively. Most events are reconstructed properly and the difference between original and reconstructed data is minor. It is clear, that after multiple removal the de-migration operator (L) can properly model the wavefield.

The common image gather (CIG) associated to CDP position 2100 of the multiple attenuated data is shown in Figure (5.10). In this CIG most event are flat. However, some events have a minor MoveOut in the mid- and far-offsets and also CIG is noisy.

In order to remove these artifacts, smoothing in the offset direction via offset dependent LS-PSTM was implemented. Figures (5.3) (c) and (d) show the effect of the aforementioned regularization for trade-off parameters $\mu = 100$ and $\mu = 2000$, respectively. Increasing the trade-off parameter causes more smoothness in the offset direction.

The effect of regularization on the resolution enhancement of LS-PSTM image is shown in Figure (5.11). Figures (5.11 a and b) show the image obtained via regularized LS-PSTM with $\mu = 100$ and $\mu = 2000$, respectively. Increasing the tradeoff parameter has removed migration artifacts and attenuated sampling noise. Subsurface layers are more continuous especially at times $> 4sec$.

Figure (5.12) shows the data reconstruction of regularized LS-PSTM for field record 647 with $\mu = 100$ and $\mu = 2000$. The difference between the original data and the re-

constructed shows that our algorithm improves the quality of the migration. However, the data reconstruction is not improved as we have introduced smoothness in the common image gather that have make the inverted model less capable of modeling the data. In other words, we have found a stable smooth solution but at the price of not honoring properly the data (overfitting) and as consequence, one is not able to model missing observations as well.

In order to measure of the difference between the reconstructed data using method of regularized LS-PSTM, and the observations in the Gulf of Mexico data set, the root-mean-square (RMS) errors is calculated for different amounts of trade-off parameter. Result is shown in Figure (5.13). The RMS error increases with increasing μ . Increasing μ may give a smooth and less noisy image of LS-PSTM, however, dose not improve the quality of data reconstruction.

5.5 Summary

In this chapter, Kirchhoff PSTM and LS-PSTM were used to study the feasibility of LSM to image and reconstruct real data. The Gulf of Mexico data set includes strong multiples which make the imaging of subsalt layers a problem.

The parabolic Radon transform was used for multiple attenuation. PSTM and regularized LS-PSTM were applied to both data with and without multiple attenuation.

As expected, PSTM and LS-PSTM should be applied to data after multiple removal. The reconstruction problem for this data is quite difficult for a time migration algorithm. It seems that using damped least squares (LS-PSTM with damping) gives more flexibility to reconstruct the data than offset dependent regularized LS-PSTM. More research is needed to find optimal regularization strategies to properly reconstruct large volumes of seismic data.

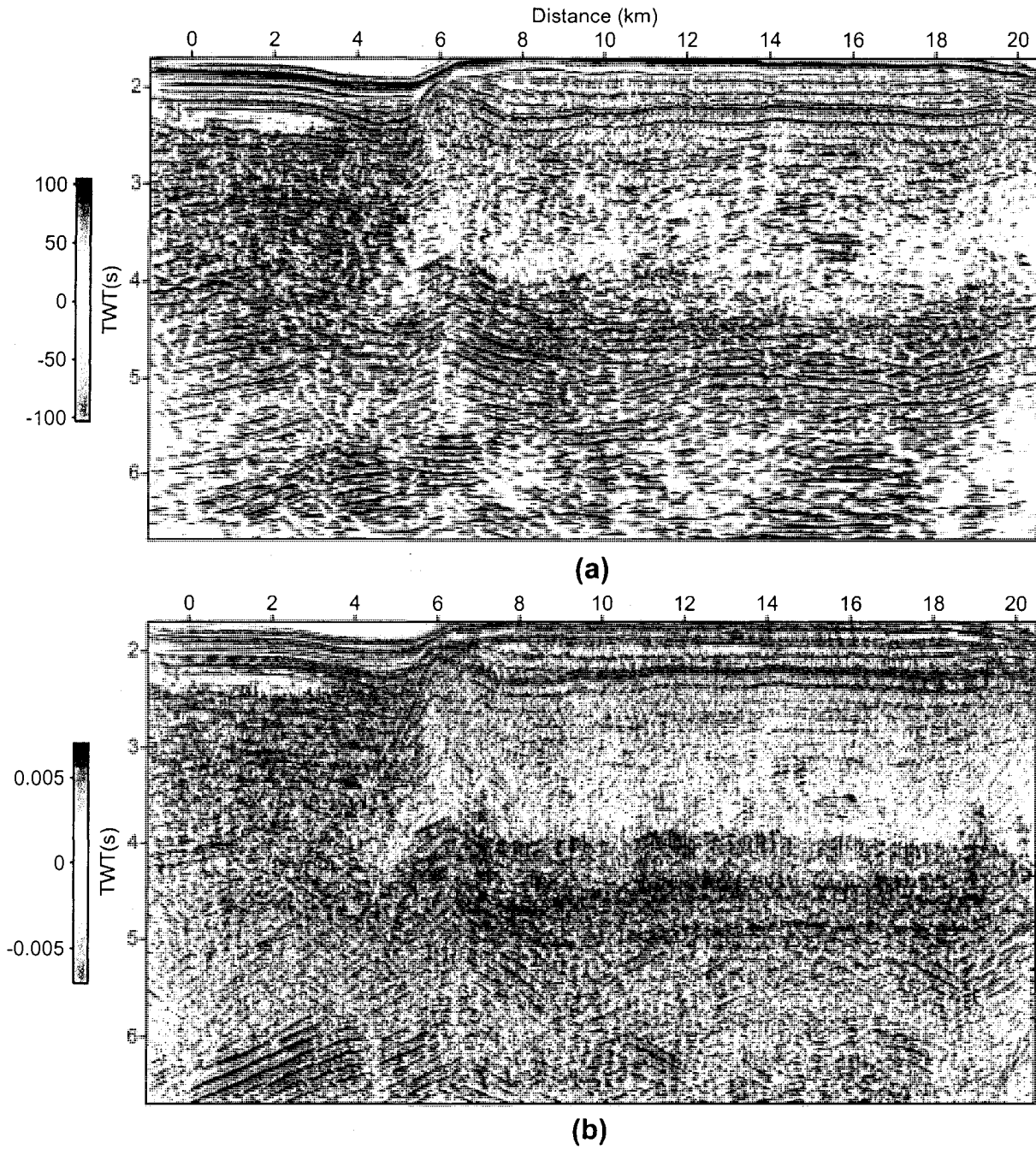


Figure 5.8: Migration images of the Gulf of Mexico data set after multiple attenuation using 50% of the shot records. a) PSTM. b) LS-PSTM.

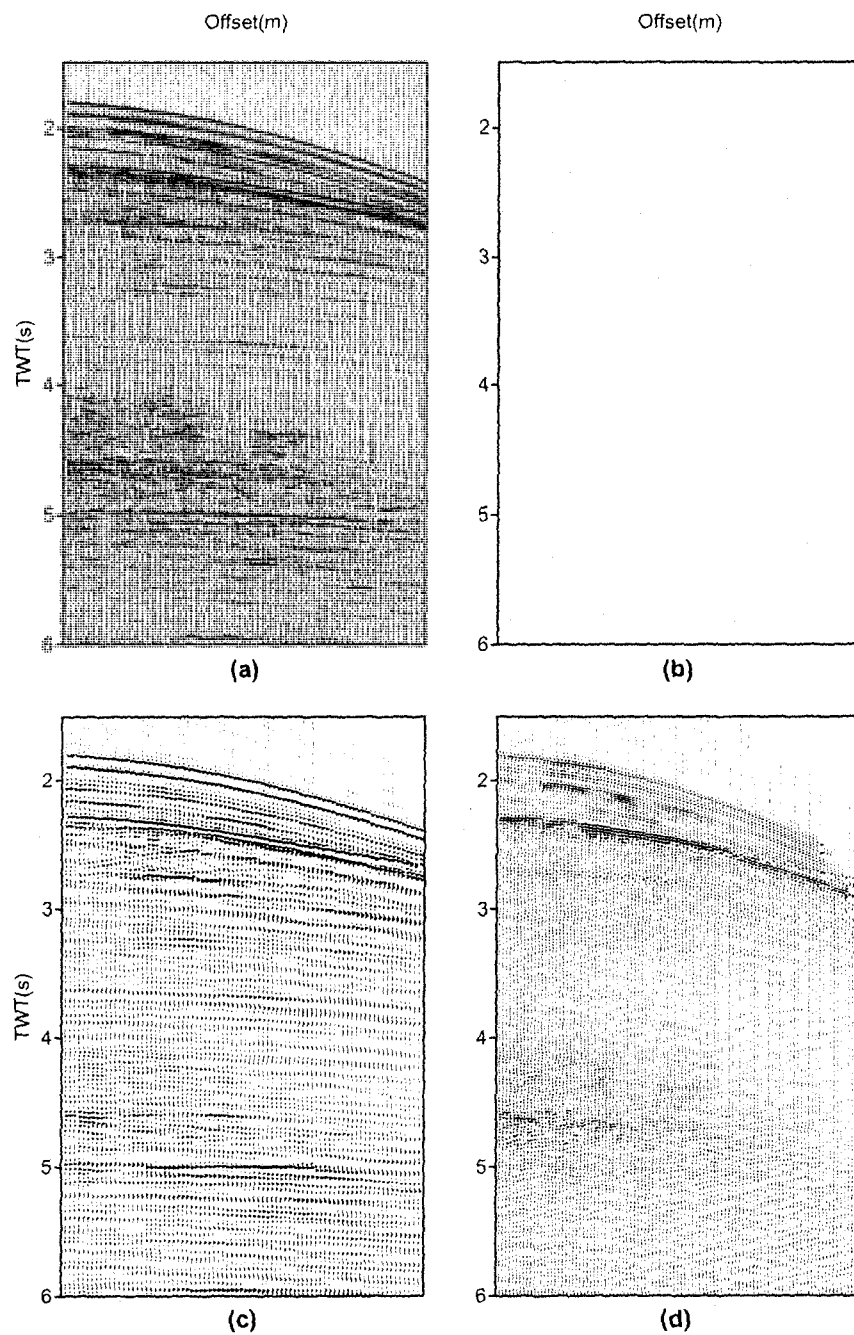


Figure 5.9: Data reconstruction of the Gulf of Mexico data set after multiple removal with parabolic Radon Transform. a) Original data. b) Decimated data c) Reconstructed data. d) Difference between original data and reconstructed data.

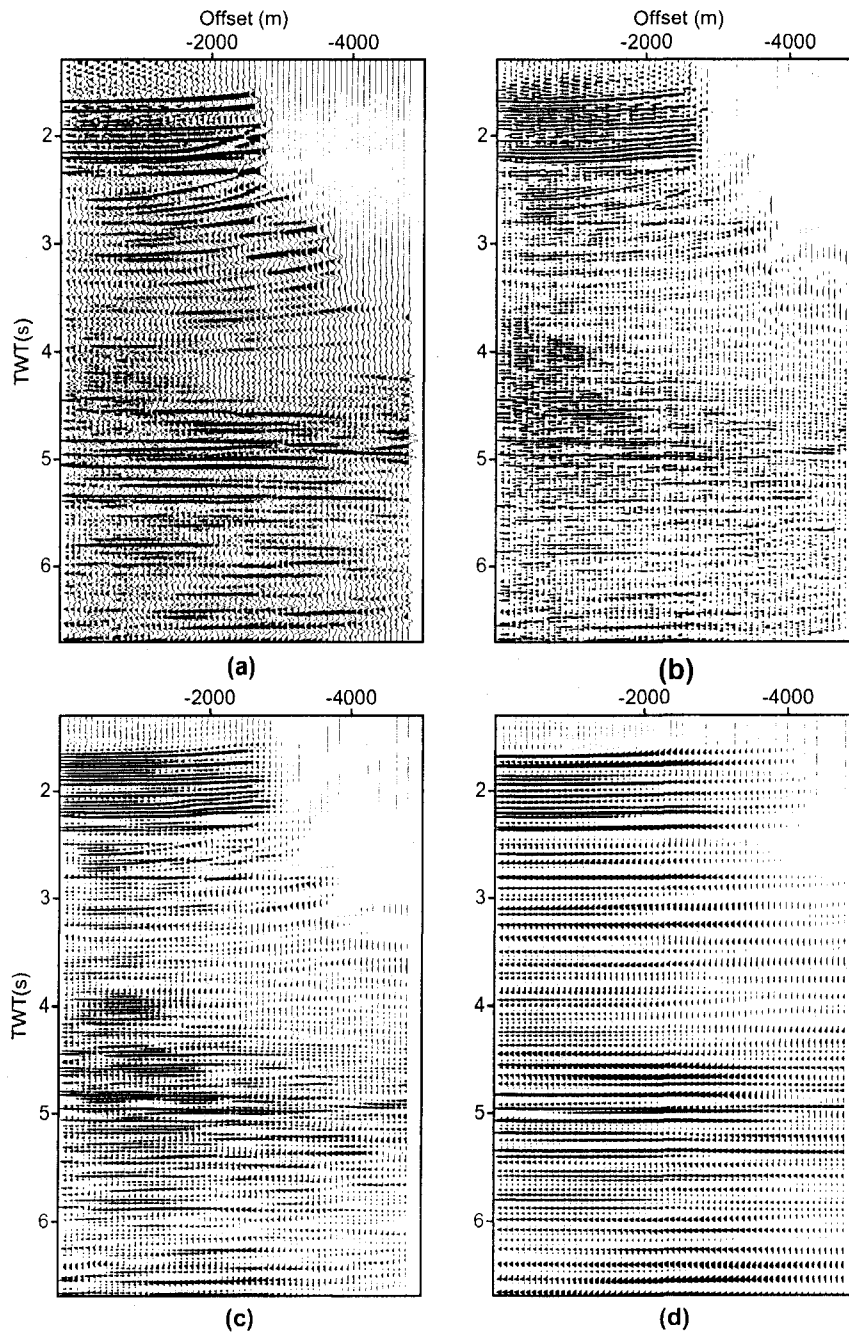
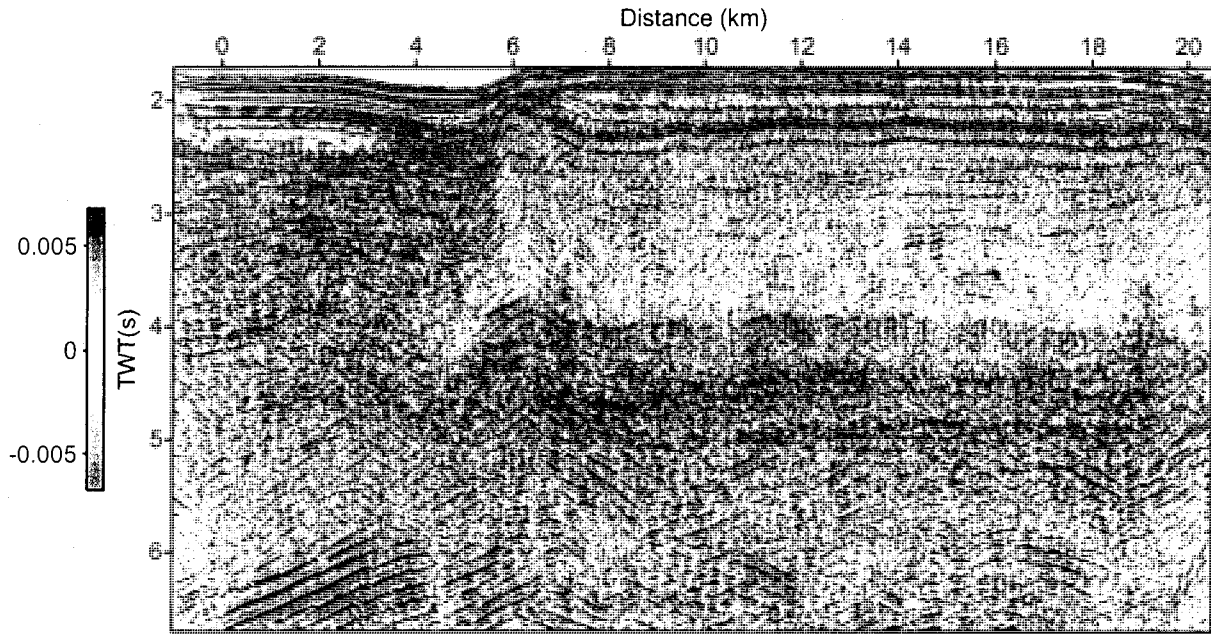
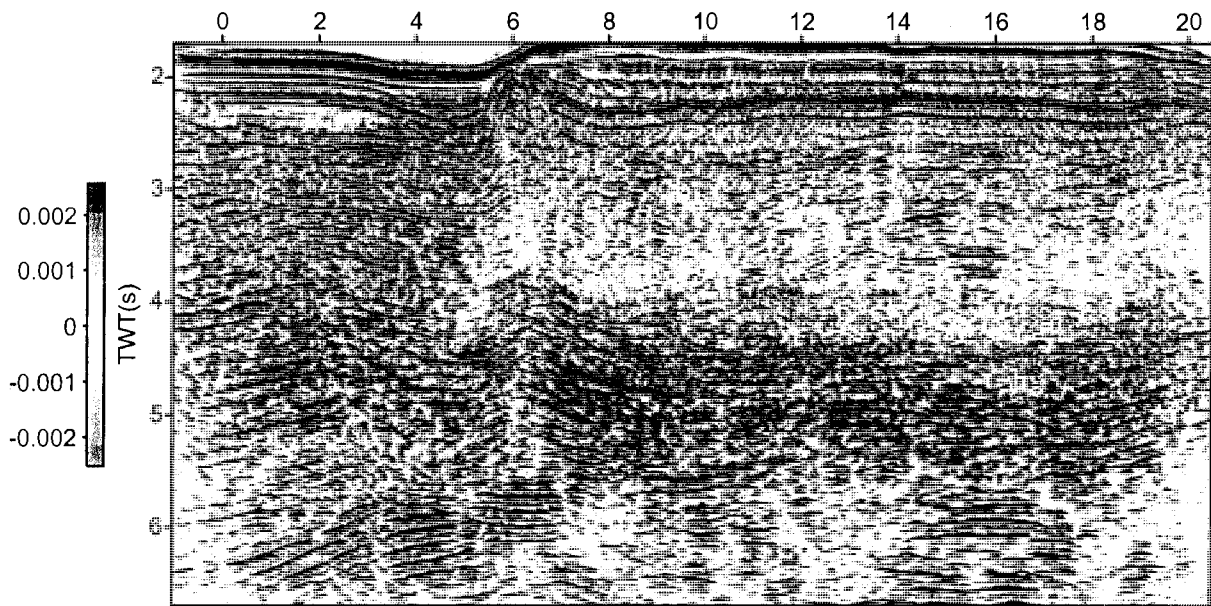


Figure 5.10: CIG of CDP 2100 from data after multiple removal. a) PSTM. b) LS-PSTM. c) LS-PSTM with offset dependent regularization with $\mu = 100$ and d) with $\mu = 2000$.



(a)



(b)

Figure 5.11: Regularized LS-PSTM images of the Gulf of Mexico data set after multiple attenuation. a) Offset dependent regularized LS-PSTM with $\mu = 100$ and . b) $\mu = 2000$.

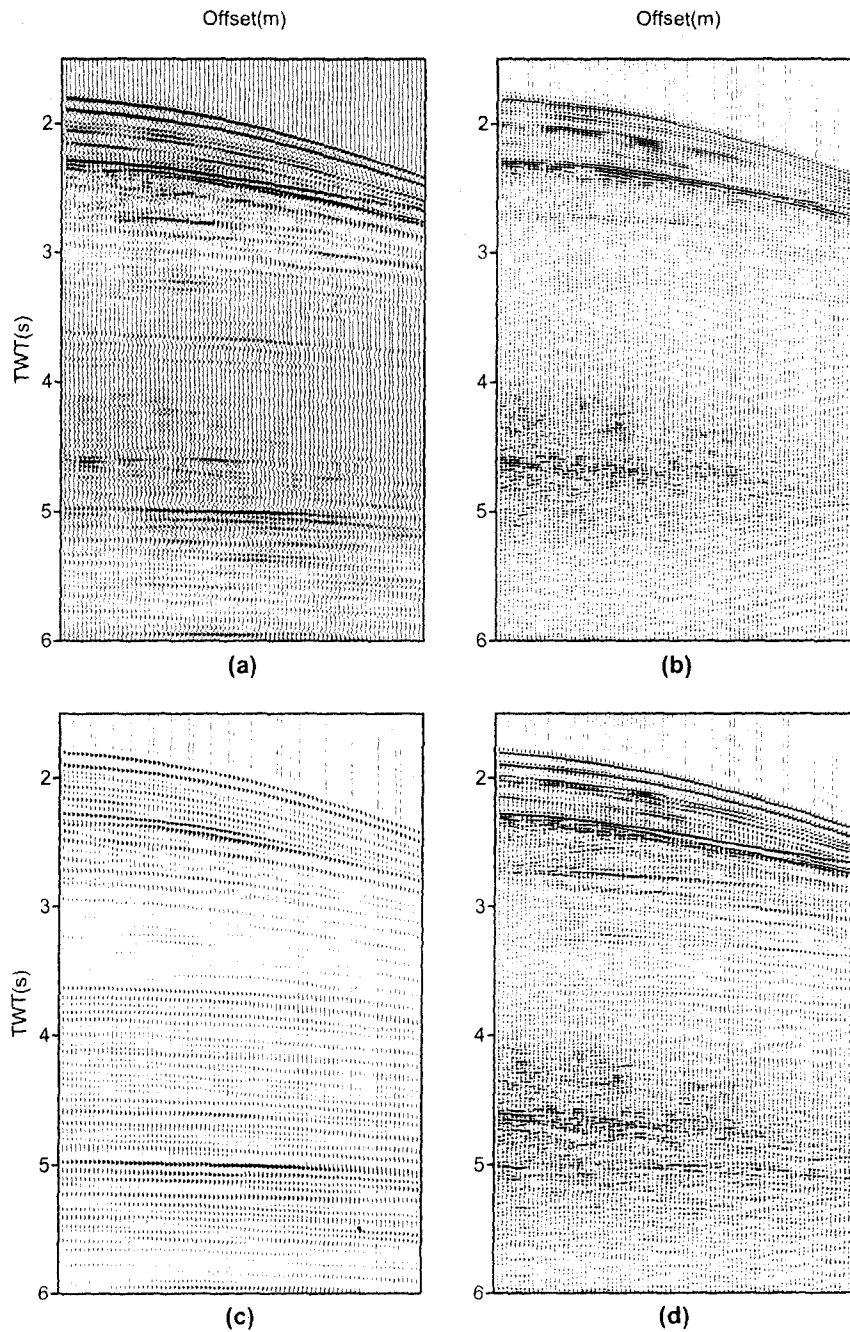


Figure 5.12: Data reconstruction of the Gulf of Mexico data set after multiple attenuation with offset dependent LS-PSTM. a) $\mu = 100$. b) Difference between original data and reconstruction with $\mu = 100$. c) Reconstructed data using regularized LS-PSTM with $\mu = 2000$. d) Difference between original data and reconstruction with $\mu = 2000$.

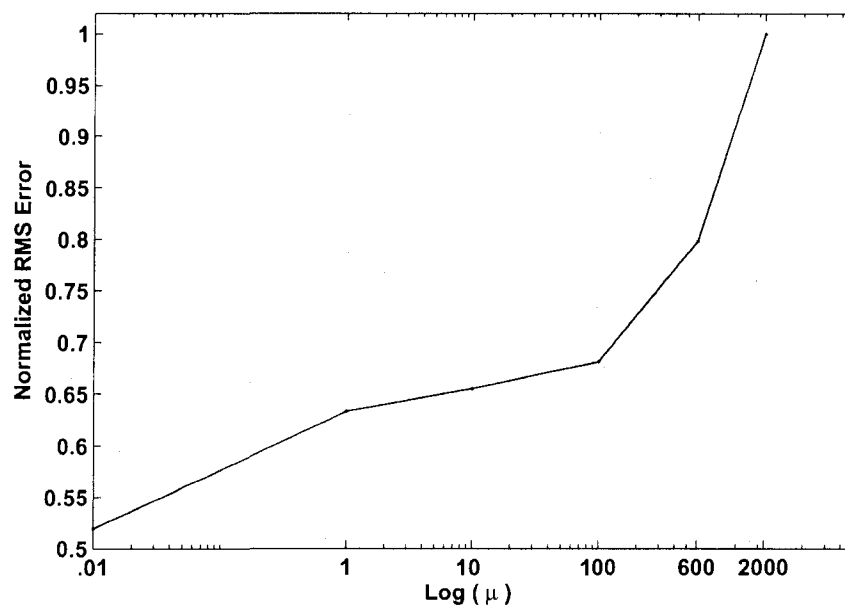


Figure 5.13: RMS error for data reconstruction by offset dependent regularized LS-PSTM for the Gulf of Mexico data set versus trade-off parameter, μ . The data reconstruction is not improved by introducing smoothness.

Chapter 6

Discussion and Conclusions

Kirchhoff PSTM is an effective tool to image seismic data and produce subsurface models. In this thesis I have investigated the problem of designing a PSTM algorithm that is able to honor prestack seismic data. The latter is achieved by posing the imaging problem as an inverse problem and trying to minimize the difference between the observed data volume and the synthetic data volume generated by the prestack de-migration operator.

The algorithm for LS-PSTM is implemented via the method of CG. I have also investigated a smoothing regularization constraint that improves the quality of CIG.

LS-PSTM was applied on two synthetic data set and one marine experiment. For the synthetic data, LS-PSTM is able to improve the quality of the subsurface reflectivity. The quality of data reconstruction is investigated as well and synthetic results leads to the conclusion that LS-PSTM can be part of our tools for regularization of seismic data in circumstances where the background velocity model is known with high accuracy.

The real data examples reveal the need to properly remove multiples prior to LS-PSTM. This is a well-known problem in seismic imaging and it is clear that constraint least-squares inversion will not be able to handle multiple reflections unless they were incorporated in the modeling operator. This is not a surprise and the test of migration prior to multiple suppression are simple added to the thesis to illustrate a well-known problem. LS-PSTM applied to data after multiple removal shows an enhancement of resolution and the ability to reconstruct the main reflections in the data. The examples with real data, as expected, are of quality well below the synthetic ones. More research in needed to make LS-PSTM robust for real world data conditions.

6.1 Future work

The results presented in this thesis can also be improved by incorporating velocity errors in the operator. There is a vast literature dealing with the problem of velocity update for prestack data (migration velocity analysis) and incorporating those concepts into LS-PSTM can lead to interesting improvements when dealing with real data.

Finally, the problem of computational cost of LS migration methods needs to be addressed. This thesis has dealt with 2D problems. In reality, 2D data is well-sampled. Acquisition problems arise in 3D surveys. It is in this case where LS-PSTM can become extremely demanding in computational needs. Consequently, preconditioning strategies to accelerate the convergence of the conjugate gradients schemes are required.

Bibliography

- Abma, R., Sun, J., and Bernitsas, N., 1999, Antialiasing methods in kirchhoff migration: *Geophysics*, **64**, no. 5, 1783–1792.
- Audebert, F., Nichols, D., Rekdal, T., Biondi, B., Lumley, D., and Urdaneta, H., 1997, Imaging complex geologic structure with single-arrival kirchhoff prestack depth migration: *Geophysics*, **62**, no. 5, 1533–1543.
- Bevc, D., and Lumley, D. E., 1994, When is anti-aliasing needed in kirchhoff migration?: *Stanford Exploration Project*, **80**, 467–476.
- Beydoun, W. B., and Mendes, M., 1989, Elastic ray-born l2-migration/inversion.: *Geophys. J.*, **97**, 151–160.
- Bleistein, N., Cohen, J. K., and Hagin, F. G., 1987, Two and one-half dimensional born inversion with an arbitrary refrence: *Geophysics*, **52**, no. 1, 26–36.
- Bleistein, N., 1984, *Mathematical methods for wave phenomena.*
- Bleistein, N., 2002, A proposal for common-opening-angle migration/inversion: CWP, Colorado School of Mines.
- Cerveny, V., 1985, The application of ray tracing to the numerical modeling of seismic wavefields in complex structure, in dohr,g.,ed., seismic shear waves: *Soc. of Expl. Geophys.*, pages 1–124.
- Chandra, R., Dagum, L., Kohr, D., Maydan, D., McDonald, J., and Menon, R., 2001, Parallel programming in openmp:.
- Claerbout, J. F., and Black, J. L., 2005, Basic earth imaging (version 2.4): Stanford Exploration Project. URL <http://sepwww.stanford.edu/sep/prof>.
- Claerbout, J. F., and Doherty, S. M., 1972, Downward continuation of moveout corrected seismograms: *Geophysics*, **37**, 741–768.
- Claerbout, J. F., 1971, Toward a unified theory of reflector mapping: *Geophysics*, **36**, 467–481.
- Claerbout, J. F., 1992, Anti-aliasing: *Stanford Exploration Project Report.*, **73**, 371–389.
- Claerbout, J. F., 2004, Earth soundings analysis: Processing versus inversion (pvi):.

BIBLIOGRAPHY

- CWP, 1984, Seismic unix: Center of Wave Phenomana, Colorado School of Mines: URL <http://www.cwp.mines.edu/cwpcodes>.
- deBruin, C., Berkhout, A. J., and Wapenaar, C., 1990, Angle dependent reflectivity by means of prestack migration: *Geophysics*, **55**, 1223–1234.
- Duquet, B., Marfurt, K. J., and Dellinger, J. A., 2000, Kirchhoff modeling, inversion for reflectivity, and subsurface illumination: *Geophysics*, **65**, 1195–1209.
- Gardner, G. H. F., and Canning, A., 1994, Effects of irregular sampling on 3d prestack migration: Expanded Abstract, 64th Annual SEG Meeting, pages 1553–1556.
- Gazdag, J., 1978, Wave equation migration with the phase-shift method: *Geophysics*, **43**, 1342–1351.
- Gray, S. H., and May, W. P., 1994, Kirchhoff migration using eikonal equation traveltimes: *Geophysics*, **59**, no. 5, 810–817.
- Gray, S. H., Etgen, J., Dellinger, J., and Whitmore, D., 2000, Seismic migration problems and solutions: *Geophysics*, **66**, no. 5, 1622–1640.
- Gray, S. H., 1992, Frequency selective design of kirchhoff migration operator: *Geophysical Prospecting*, **40**, 565–571.
- Gulunay, N., 2003, Seismic trace interpolation in the fourier transform domain: *Geophysics*, **68**, no. 1, 355–369.
- Hagedoorn, J. G., 1954, A process of seismic reflection interpretation: *Geophysical Prospecting*, **2**, 85–127.
- Hampson, D., 1986, Inverse velocity stacking for multiple elimination: *Journal of the Canadian Society of Exploration Geophysicists*, **22**, 44–55.
- Hertweck, T., Jager, C., Goertz, A., and Schleicher, J., 2003, Aperture effects in 2.5d kirchhoff migration: A geometrical explanation: *Geophysics*, **68**, no. 5, 1673–1684.
- Hestenes, M., and Steifel, E., 1952, Methods of conjugate gradients for solving linear systems: *Nat. Bur. Standards J. Res.*, **49**, 403–436.
- Jin, S., Madariaga, R., Virieux, J., and Lambare, G., 1992, Two-dimensional asymptotic iterative elastic inversion: *Geophys. J. Int.*, **108**, 575–588.
- Kuehl, H., and Sacchi, M. D., 2001a, Generalized least-squares dsr migration using a common angle imaging condition: 71st Ann. Intranet. Mtg. Soc. Expl. Geophys. Expanded Abstracts, MIG 4.4.
- Kuehl, H., and Sacchi, M. D., 2001b, Split-step wkbj least-squares migration/inversion of incomplete data: 5th Soc. Expl. Geophys. of Japan Internat. Symp. Imaging Technology.
- Kuehl, H., and Sacchi, M. D., 2003, Least-squares wave-equation migration for avp/ava inversion: *Geophysics*, **68**, no. 1, 262–273.
- LeBras, R., and Clayton, R., 1988, A iterative inversion of back-scattered acoustic waves: *Geophysics*, **53**, 501–508.

BIBLIOGRAPHY

- Liu, Z., 1996, Multiple removal by least-squares migration filtering: Univ. of Utah, Tomography and Modeling/Migration Development Project, Annual Report, pages 291–309.
- Lumley, D. E., and Beydoun, W. B., 1997, Elastic parameter estimation by kirchhoff prestack depth migration/inversion: SEP Report, 70, 162–190.
- Lumley, D. E., Claerbout, J. F., and Bevc, D., 1994, Anti-aliased kirchhoff 3-d migration: Expanded Abstract, 64th Annual SEG Meeting, pages 1282–1285.
- Lumley, D. E., 1989, Kirchhoff prestack depth migration: Imaging conditions and amplitude recovery: Expanded Abstract, 59th Annual SEG Meeting, pages 1336–1339.
- Menke, W., 1989, Geophysical data analysis: discrete inverse theory: Academic Press, 45.
- Moldoveanu, C., 2006, Coherent noise attenuation using radon transform: MSc thesis, University of Alberta, pages 31–32.
- Morse, P. M., and Feshbak, H., 1953, Method of theoretical physics, parts i and ii: New York, McGraw-Hill Book Co., Inc, I, 834.
- Nemeth, T., Wu, C., and Schuster, G. T., 1999, Least-squares migration of incomplete reflection data: Geophysics, 64, no. 1, 208–221.
- Nemeth, T., Sun, H., and Schuster, G. T., 2000, Separation of signal and coherent noise by migration filtering: Geophysics, 65, no. 2, 574–583.
- Porsani, M., 1999, Seismic trace interpolation using half-step prediction filters.: Geophysics, 64, no. 5, 1461–1467.
- Rastogi, R., and Phadke, S., 2002, Optimal aperture width selection and parallel implementation of kirchhoff migration algorithm: SPG 4th Conference and Exposition on petroleum geophysics, Mumbai, India.
- Reshet, M., and Kosloff, D., 1986, Migration of common shotgathers: Geophysics, 51, 324–331.
- Sacchi, M. D., Wang, J., and Kuehl, H., 2006, Regularized migration/inversion: New generation of seismic imaging algorithms: CSEG Recorder, Special Edition, pages 54–59.
- Scales, J., 1987, Tomographic inversion via the conjugate gradient methods: Geophysics, 52, 179–185.
- Schleicher, J., Hubral, P., Tygel, M., and Jaya, M. S., 1997, Minimum apertures and fresnel zones in migration and demigration: Geophysics, 62, no. 1, 183–194.
- Schneider, W. A., 1978, Integral formulation for migration in two-dimensions and three-dimensions: Geophysics, 43, 49–76.
- Sheriff, R. E., 1980, Nomogram for fresnel zone calculation: Geophysics, 45, 968–994.
- Spitz, S., 1991, Seismic trace interpolation in the $f - x$ domain: Geophysics, 56, no. 6, 785–796.

BIBLIOGRAPHY

- Stolt, R. H., 1978, Migration by fourier transform: *Geophysics*, **43**, 23–48.
- Strang, G., 1986, *Introduction to applied mathematics*: Wellesley-Cambridge Press.
- Sun, S., and Bancroft, J. C., 2001, How much does the migration aperture actually contribute to the migration result?: Expanded Abstract, Annual SEG Meeting, San Antonio, Texas, pages 973–976.
- Tarantola, A., 1984, Inversion of seismic reflection data in the acoustic approximation: *Geophysics*, **49**, no. 8, 1259–1266.
- Tikhonov, A., 1963, Solution of incorrectly formulated problems and the regularization method: *Soviet Math Dokl*, , no. 4, 1035–1038.
- Versteeg, R. J., 1993, Sensitivity of prestack depth migration to the velocity model: *Geophysics*, **58**, no. 6, 873–882.
- Vidale, J., 1988, Finite-difference calculation of traveltimes: *Bull. Seis. Soc. Am.*, **78**, 2062–2076.
- Vreschuur, D. J., and Prein, R. J., 1999, Multiple removal from delft university: *The Leading Edge*, **18**, no. 1, 86–91.
- Wang, J., and Sacchi, M. D., 2007, High-resolution wave-equation amplitude-variation-with-ray-parameter (avp) imaging with sparseness constraints: *Geophysics*, **72**, no. 1, s11–s18.
- Wang, J., 2005, 3-d least-squares wave-equation avp/ava migration of common azimuth data: PhD thesis, University of Alberta, pages 70–74.
- Weglein, A. B., 1999, Multiple attenuation: an overview of recent advances and the road ahead: *The Leading Edge*, **18**, no. 1, 40–44.
- Xu, S., Chauris, H., Lambare, G., and Noble, M., 2001, Common-angle migration: A strategy for imaging complex media: *Geophysics*, **66**, 1877–1894.
- Zhang, Y., Gray, S., and Young, J., 2000, Exact and approximate weights for kirchhoff migration: Expanded Abstract, Annual SEG Meeting, pages 1036–1039.